

Three flavor long-wavelength vacuum oscillation solution to the solar neutrino problem

A. M. Gago*

*Instituto de Física, Universidade de São Paulo C. P. 66.318, 05315-970 São Paulo, Brazil
and Sección Física, Departamento de Ciencias, Pontificia Universidad Católica del Perú, Apartado 1761, Lima, Perú*

H. Nunokawa†

Instituto de Física Gleb Wataghin, Universidade Estadual de Campinas, UNICAMP 13083-970 – Campinas, Brazil

R. Zukanovich Funchal‡

*Instituto de Física, Universidade de São Paulo C. P. 66.318, 05315-970 São Paulo, Brazil
(Received 6 June 2000; revised manuscript received 19 July 2000; published 6 December 2000)*

We investigate the current status of the long-wavelength vacuum oscillation solution to the solar neutrino problem and to what extent the presence of a third neutrino can affect and modify it. Assuming that the smaller mass squared difference that can induce such oscillations Δm_{12}^2 is in the range $10^{-11} - 10^{-8} \text{ eV}^2$ and the larger one, Δm_{23}^2 , in the range relevant to atmospheric neutrino observations, we analyze the most recent solar neutrino data coming from Homestake, SAGE, GALLEX, GNO, and Super-Kamiokande experiments in the context of three neutrino generations. We include in our vacuum oscillation analysis the Mikheyev-Smirnov-Wolfenstein (MSW) effect in the Sun, which is relevant for some of the parameter space scrutinized. We have also performed, as an extreme exercise, the fit without Homestake data. While we found that the MSW effect basically does not affect the best fitted parameters, it significantly modifies the allowed parameter space for Δm_{12}^2 larger than $\sim 3 \times 10^{-10} \text{ eV}^2$, in good agreement with the result obtained by Friedland in the case of two generations. Although the presence of a third neutrino does not essentially improve the quality of the fit, the solar neutrino data alone can give an upper bound on θ_{13} , which is constrained to be less than $\sim 60^\circ$ at 95 % C.L.

DOI: 10.1103/PhysRevD.63.013005

PACS number(s): 14.60.Pq

I. INTRODUCTION

The solar neutrino problem (SNP) [1] seems now to be established as a definite signal of nonstandard neutrino properties by the four first generation solar neutrino experiments Homestake [2], Kamiokande [3], GALLEX [4], SAGE [5], and by the new generation higher statistics solar neutrino experiments Super-Kamiokande [6] and GNO [7], which have strengthened the existence of the SNP. Astrophysical explanations of the SNP, which require significant deviation from the standard solar model (SSM) [8,9], are highly excluded with the current solar neutrino data [10]. Moreover, there is an excellent agreement between the sound velocity predicted by the SSM and that obtained from the recent helioseismological observations [11], which supports the rigidity of the SSM.

Albeit electron neutrinos, produced in the Sun, most certainly vanish on their way to the Earth, which is the dynamical origin of the process, their disappearance is yet to be completely clarified. It has been discussed that the SNP can be nicely explained by the simplest extension of the standard electroweak model which invokes neutrino mass and flavor mixing [12]. The most plausible solutions in this context are provided either by the matter enhanced resonant neutrino conversion, the Mikheyev-Smirnov-Wolfenstein (MSW) ef-

fect [13], or by the vacuum oscillation [14] with a typical wavelength as long as the Sun-Earth distance [15]. Recent detailed analyses and discussions of the solar neutrino data based on these mechanisms, i.e., the MSW and long-wavelength vacuum oscillation (LVO) solutions, in the context of two neutrino generations, can be found in Refs. [16,17] and Refs. [16,18], respectively. Earlier detailed analyses, prior to the Super-Kamiokande experimental results, can be found in Refs. [19,20]. Discussions of other possibilities to explain the SNP by invoking more exotic properties such as the neutrino magnetic moment, flavor changing interactions or violation of the equivalence principle, can be found, for example, in Ref. [21].

Although it seems at present that pure $\nu_\mu \rightarrow \nu_\tau$ oscillations in vacuum are quite enough to account for the atmospheric neutrino anomaly [22,23], the possibility of having contributions from non-negligible $\nu_\mu \rightarrow \nu_e$ oscillations is still not discarded [24,25], even after taking into account the constraints coming from the CHOOZ reactor experiment [26]. Moreover, the existence of at least three neutrino flavors, which is one of the most impressive results from the CERN e^+e^- collider LEP experiments [27,28], makes it unavoidable to try to understand neutrino oscillations in a full three generation scenario.

In the framework of three generations of massive neutrinos subjected to flavor mixing, one has to deal, in general, with six variables to study the neutrino oscillation phenomena, namely, three mixing angles θ_{12} , θ_{23} , θ_{13} and one CP violating phase δ , which relate mass and flavor eigenstates, and two (independent) mass squared differences, which can

*Email address: agago@charme.if.usp.br

†Email address: nunokawa@ifi.unicamp.br

‡Email address: zukanov@charme.if.usp.br

TABLE I. Solar neutrino rates observed by Homestake, SAGE, and GALLEX/GNO combined as well as theoretical predictions for the the standard solar model by Bahcall and Pinsonneault [8]. For SK we show the ratio of the observed flux over the prediction of the BP98 SSM.

Experiment	Observed Rate	Ref.	BP98 SSM Predictions [8]	Units
Homestake	2.56 ± 0.23	[2]	$7.7^{+1.2}_{-1.0}$	SNU
SAGE	75.4 ± 7.6	[5]	129^{+8}_{-9}	SNU
GALLEX/GNO	74.1 ± 6.8	[4,7]	129^{+8}_{-9}	SNU
Super-Kamiokande	0.465 ± 0.015	[6]	$1.00^{+0.19}_{-0.14}$	$5.15 \times 10^6 \text{ cm}^{-2} \text{ s}^{-1}$

be chosen as $\Delta m_{12}^2 \equiv m_2^2 - m_1^2$ and $\Delta m_{23}^2 \equiv m_3^2 - m_2^2$. If we assume that the smaller mass squared difference, defined as Δm_{12}^2 , is in the range relevant to solar neutrino oscillation, i.e., $\Delta m_{12}^2 \sim 10^{-11} - 10^{-8} \text{ eV}^2$ in the case of the LVO solution or $\Delta m_{12}^2 \sim 10^{-8} - 10^{-5} \text{ eV}^2$ in the case of the MSW solution, and the larger one, Δm_{23}^2 , is in the range relevant to the atmospheric neutrino observations, i.e., $\Delta m_{23}^2 \sim 10^{-3} - 10^{-2} \text{ eV}^2$, only three of these variables become significant in practice to the solar neutrino investigation: θ_{12} , θ_{13} , and Δm_{12}^2 [29–31].

Under such an assumption, a detailed analysis of the three flavor LVO solution to the SNP was performed in Ref. [32] in which the best fit was obtained when θ_{13} is zero, this angle being constrained to be less than $\sim 30^\circ$ at 95 % C.L. by the solar neutrino data alone. The authors of Ref. [32] have in addition taken into account the atmospheric neutrino results, and found that the combined three generation fit does not lead to an allowed region appreciably different from the one obtained by performing two separate effective two-neutrino fits to the solar and atmospheric neutrino data. See, for instance, Ref. [33] for earlier discussions on the three flavor LVO solution to the SNP.

On the other hand, a detailed three flavor analysis of the MSW solution to the SNP was performed in Ref. [34] and not long ago its updated version was reported in Ref. [35]. The best fit obtained by this study permitted us to constrain $\theta_{13} \lesssim 55^\circ - 60^\circ$ at 95 % C.L. by the solar neutrino data on its own, without taking into account the atmospheric neutrino observations [22] or the CHOOZ result [26]. More recently, a complete analysis considering four neutrinos, three active and one sterile, was performed in the context of MSW as well as LVO oscillation solutions [36], and bounds on mixing angles were again obtained solely by the solar neutrino data.

In this same spirit we reexamine and update in this paper the long-wavelength vacuum oscillation solution to the SNP in the two generation as well as in the three generation frameworks. In this study, we do not take into account the constraints on θ_{13} coming from the Super-Kamiokande atmospheric neutrino observations [22] nor by the CHOOZ reactor experiment [26], whose combination gives an upper bound on θ_{13} corresponding to $\sin^2 \theta_{13} \lesssim \text{few } \%$ [24,25]. The main idea of this paper is to constrain θ_{13} by LVO and the solar neutrino data alone, as has already been done for the atmospheric neutrino [24,25] and MSW solar neutrino solutions [35].

Moreover, we investigate the effect of taking the ^8B neu-

trino flux as known only up to a normalization factor f_B renormalizing, in this case, the ^7Be flux accordingly, assuming the solar temperature power law [37]. Finally, we also perform an extreme check analysis by neglecting completely the solar neutrino rate measured by the Homestake experiment, as considered, for instance, in Ref. [38], on the account of it being the only radiochemical experiment which has not been calibrated with a radioactive source.

There are new ingredients we include in this work, which were not considered in previous analyses of the three flavor LVO solution. We extend the analysis to mass squared differences up to 10^{-8} eV^2 in order to cover the whole relevant LVO parameter space. Above this value the oscillation probability of solar neutrinos essentially does not depend on the distance between the Sun and the Earth as discussed in Ref. [39], and we do not regard such case as a LVO solution to the SNP. Thereby, we include in our estimations the MSW effect in the Sun in the context of the LVO solution, whose importance was first pointed out in Ref. [40] for $\Delta m_{12}^2/E$ larger than $3 \times 10^{-10} \text{ eV}^2/\text{MeV}$. The relevance of the MSW effect in determining the LVO allowed parameter space has been recently discussed in Ref [41]. Due to the presence of a matter effect, we cover the whole relevant range of mixing angle $0 \leq \theta_{12} \leq \pi/2$ [41] in contrast to the range usually considered ($0 \leq \theta_{12} \leq \pi/4$) for the LVO solution.

We have used in our analysis the most recent solar neutrino data from the five solar neutrino experiments:¹ the total rates measured by the Homestake chlorine (Cl) detector [2], by the GALLEX [4], GNO [7], and SAGE [5] gallium (Ga) detectors, which are summarized in Table I, as well as all the observations performed by the high-statistics Super-Kamiokande (SK) water Cherenkov detector (total rate, energy spectrum, and zenith angle dependence) [6]. The pioneering Homestake experiment which has its energy threshold at $E_\nu = 0.814 \text{ MeV}$ [1] is mostly sensitive to ^8B neutrinos ($\sim 76\%$ of the total contributions), and also can detect ^7Be neutrinos ($\sim 15\%$). The gallium detectors have their threshold at $E_\nu = 0.233 \text{ MeV}$ [1] and are sensitive to pp ($\sim 54\%$), ^7Be ($\sim 27\%$), and also to ^8B neutrinos ($\sim 10\%$). Super-Kamiokande which has its energy threshold at $E_e = 5.5 \text{ MeV}$, where E_e is the total energy of the recoil

¹For the sake of simplicity, we have not included the data from the Kamiokande experiment [3], which can be justified by the fact that its result is consistent with that of SK and its errors are much larger than that of the SK experiment.

electron, is only sensitive to ^8B neutrinos.²

This paper is organized as follows. In Sec. II we present the oscillation formalism we will use to pave the way to the two and three neutrino generation analyses of the data. In Sec. III we present and discuss the general features of our data analysis. In Sec. IV we revise and update the two-generation LVO solution also including the MSW effect in the Sun. In Sec. V we extend the analysis to three-generation neutrino oscillation taking into account the MSW effect. In Sec. VI we examine the seasonal effect that can be expected at SK, Borexino, and KamLAND experiments for the best fitted parameters of the LVO solutions we found. In Sec. VII we discuss the LVO solution with two and three neutrino flavors disregarding the chlorine data. Finally we draw our conclusions in Sec. VIII.

II. OSCILLATION FORMALISM

In this section we describe the framework we will use in the scope of this paper.

A. Two flavor case

For the two generation case in which ν_e is mixed only with ν_μ (the same argument holds also for the case of ν_e - ν_τ mixing), the evolution equation of neutrino traveling through matter can be written as

$$i \frac{d}{dx} \begin{bmatrix} \nu_e \\ \nu_\mu \end{bmatrix} = \begin{bmatrix} V_e(x) & \frac{1}{2} \Delta_{12} \sin 2\theta_{12} \\ \frac{1}{2} \Delta_{12} \sin 2\theta_{12} & \Delta_{12} \cos 2\theta_{12} \end{bmatrix} \begin{bmatrix} \nu_e \\ \nu_\mu \end{bmatrix}, \quad (1)$$

where $\Delta_{12} \equiv \Delta m_{12}^2 / 2E$, with the mass squared difference of the two neutrino mass eigenstates $\Delta m_{12}^2 = m_2^2 - m_1^2$, E is the neutrino energy, θ_{12} is the mixing angle, and

$$V_e(x) \equiv \sqrt{2} G_F N_e(x) \approx 7.6 \times 10^{-14} \times \left[\frac{N_e}{1 \text{ mol/cc}} \right] \text{ eV} \quad (2)$$

is the matter potential for ν_e with G_F and N_e being the Fermi constant and the electron number density, respectively.

This equation, in the case of vacuum ($V_e = 0$), simplifies to lead to the well-known formula for the ν_e survival probability,

$$\begin{aligned} P_{2\text{g,vac}}(\nu_e \rightarrow \nu_e) &= 1 - \sin^2 2\theta_{12} \sin^2 \left(\frac{\Delta_{12}}{2} L \right) \\ &= 1 - \sin^2 2\theta_{12} \sin^2 \left(1.27 \left[\frac{\Delta m_{12}^2}{\text{eV}^2} \right] \right. \\ &\quad \left. \times \left[\frac{\text{MeV}}{E} \right] \left[\frac{L}{\text{m}} \right] \right), \end{aligned} \quad (3)$$

²In this work, we do not take into account the possible enhancement of hep neutrinos [42] in the SK spectrum analysis since the current SK data do not seem to agree on the necessity of such an enhancement [6].

where L is the distance traveled by the neutrino. It is clear that the probability $P_{2\text{g,vac}}$ is invariant under the transformation $\Delta m_{12}^2 \rightarrow -\Delta m_{12}^2$ as well as $\theta_{12} \rightarrow \pi/2 - \theta_{12}$ and therefore, in vacuum it is sufficient to assume $\Delta m_{12}^2 > 0$ and $0 \leq \theta_{12} \leq \pi/4$ to account for all physical situations.

From Eq. (3) we can estimate the vacuum oscillation length as

$$\begin{aligned} L_{\text{osc}} &= \frac{4\pi E}{\Delta m_{12}^2} \approx 2.47 \times 10^{10} \left[\frac{E}{1 \text{ MeV}} \right] \left[\frac{10^{-10} \text{ eV}^2}{\Delta m_{12}^2} \right] \text{ m} \\ &\approx 0.165 L_0 \left[\frac{E}{1 \text{ MeV}} \right] \left[\frac{10^{-10} \text{ eV}^2}{\Delta m_{12}^2} \right], \end{aligned} \quad (4)$$

where $L_0 \equiv 1 \text{ AU} \approx 1.496 \times 10^{11} \text{ m}$, is the astronomical unit, namely, the mean Earth-Sun distance.

If matter is present, the physics described by the neutrino evolution given in Eq. (1) is not invariant under either transformation $\Delta m_{12}^2 \rightarrow -\Delta m_{12}^2$ or $\theta_{12} \rightarrow \pi/2 - \theta_{12}$. However, we can show that the physical consequence of Eq. (1) is invariant under the transformation $\theta_{12} \rightarrow \pi - \theta_{12}$ as well as $(\Delta m_{12}^2, \theta_{12}) \rightarrow (-\Delta m_{12}^2, \pi/2 - \theta_{12})$. Therefore, in order to cover all the possible physically meaningful parameter region we can assume [34,35]

$$\Delta m_{12}^2 > 0, \quad 0 \leq \theta_{12} \leq \frac{\pi}{2}. \quad (5)$$

This is the range we consider in this work. In principle, neutrinos on their way from the interior of the Sun to the detector on the Earth can be influenced by the solar as well as by the Earth matter potentials.

Let us initially consider what can happen in the Sun. In Fig. 1(a) we show the isosurvival probability contours of ν_e at the solar surface as a function of $\Delta m_{12}^2/E$ and $\sin^2 \theta_{12}$ for pure vacuum oscillation, ignoring the matter effect, assuming that neutrinos are created in the solar center. In Fig. 1(b) we show the same type of contours but taking into account the matter effect. The probabilities were obtained by numerically integrating Eq. (1), using the electron number density one can find in Ref. [43], again assuming that neutrinos are created in the center of the Sun.

From these two plots, we immediately see that the probability at the solar surface can be significantly different for these two cases if $\Delta m_{12}^2/E \geq \text{few} \times 10^{-10} \text{ eV}^2/\text{MeV}$. Therefore, one can not disregard the matter influence in the ν_e survival probability calculation for values of $\Delta m_{12}^2/E$ in this range. For smaller values of $\Delta m_{12}^2/E$ the oscillation effect is small and the survival probabilities are ~ 1 , in both cases. For $\Delta m_{12}^2/E \sim \mathcal{O}(10^{-9}) \text{ eV}^2/\text{MeV}$ or smaller, the role of the solar matter is to suppress oscillations, as $\Delta m_{12}^2/E$ increases the MSW resonance effect comes into play and strong conversion can occur. We note that for values of $\Delta m_{12}^2 \geq 10^{-9} \text{ eV}^2$, the MSW conversion can be significant for lower energy neutrinos, such as pp and ^7Be ones, but it will be very weak for most of the ^8B neutrinos. In fact, we can see from Fig. 1(b), that even for $\Delta m_{12}^2 = 10^{-8} \text{ eV}^2$, the

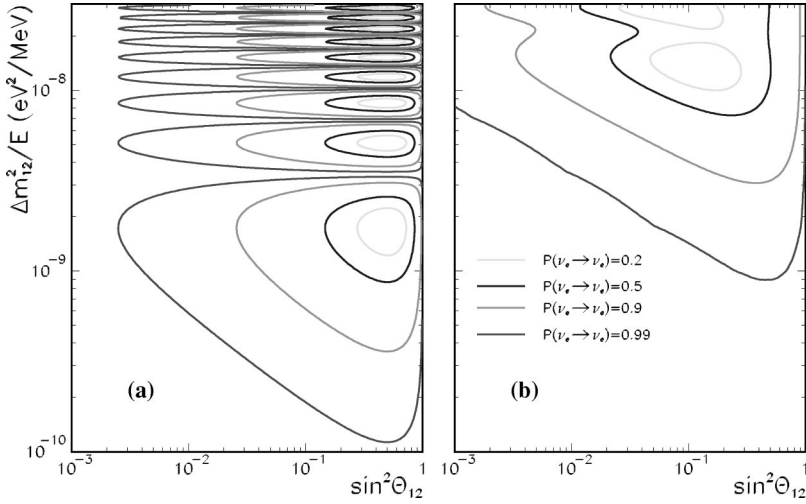


FIG. 1. Contours of isosurvival probability of ν_e at the surface of the Sun as a function of $\Delta m_{12}^2/E$ and $\sin^2 \theta_{12}$ (a) considering pure vacuum oscillation and (b) when matter is taken into account. For the case (b) we numerically integrated the evolution Eq. (1) assuming that neutrinos are created at the center of the Sun.

highest value considered in this work, if we take $E \sim 10$ MeV, the typical ${}^8\text{B}$ neutrino energy relevant for SK, the survival probability of ν_e at the solar surface is very close to 1. This implies that at such high energies, neutrinos exit from the Sun essentially as ν_e .

Let us now examine what happens in the Earth. For the averaged electron number density found in the Earth's mantle ($N_e \sim 2$ mol/cc) or core ($N_e \sim 5$ mol/cc), the matter potential V_e is always much larger than Δ_{12} , unless Δm_{12}^2 is very close to 10^{-8} eV² for the lowest energy (i.e., pp) neutrinos [see Eq. (2)], leading to a strong suppression of the effective mixing angle in the Earth matter. This implies that no appreciable $\nu_{\mu,\tau} \rightarrow \nu_e$ (or $\nu_e \rightarrow \nu_{\mu,\tau}$) regeneration effect can occur in the Earth, since this can promote, at the most, a few % change in the probability for a very limited range of mixing parameters ($\Delta_{12} \sim 10^{-7}$ eV²/MeV and large θ_{12}). Hence, in this work we only take into account the MSW effect in the Sun and neglect it completely in the Earth.

After accounting for the MSW effect in the Sun, the ν_e survival probability at the Earth given in Eq. (3) is modified as follows [40]:

$$\begin{aligned}
P_{2g}(\nu_e \rightarrow \nu_e) &= \cos^2 \theta_{12} |A_{\nu_1}(R_\odot)|^2 + \sin^2 \theta_{12} |A_{\nu_2}(R_\odot)|^2 \\
&\quad + \sin 2 \theta_{12} |A_{\nu_1}(R_\odot) A_{\nu_2}(R_\odot)| \cos(\Delta_{12} L + \beta),
\end{aligned} \tag{6}$$

where $A_{\nu_1}(R_\odot)$ and $A_{\nu_2}(R_\odot)$ are, respectively, the amplitudes of the neutrino state to be found in the mass eigenstate ν_1 and ν_2 at the solar surface, L is the distance between the solar surface and the detection point, and $\beta \equiv \text{Arg}[A_{\nu_1}(R_\odot) A_{\nu_2}^*(R_\odot)]$ corresponds to the phase developed between ν_1 and ν_2 after the neutrinos pass the resonance point until they reach the solar surface. We remark that for the values of Δm_{12}^2 we are interested in this work, in the region where ν_e 's are created, typically $r \leq 0.3 R_\odot$, because of the condition $V_e \gg \Delta_{12}$, they essentially coincide with the mass eigenstate ν_2 ($\sim \nu_e$), and no oscillation occurs within this region. Hence the final probability amplitudes

$A_{\nu_1}(R_\odot)$ and $A_{\nu_2}(R_\odot)$ as well as β do not depend on the exact production point, allowing us to assume that all neutrinos are created in the solar center [40].

The probability in Eq. (6) can be rewritten in terms of the flavor amplitudes as

$$\begin{aligned}
P_{2g}(\nu_e \rightarrow \nu_e) &= |A_{\nu_e}(R_\odot)|^2 \left[1 - \sin^2 2 \theta_{12} \sin^2 \left(\frac{\Delta_{12} L}{2} \right) \right] + |A_{\nu_x}(R_\odot)|^2 \\
&\quad \times \sin^2 2 \theta_{12} \sin^2 \left(\frac{\Delta_{12} L}{2} \right) - \sin 2 \theta_{12} |A_{\nu_e}(R_\odot) A_{\nu_x}(R_\odot)| \\
&\quad \times \left[2 \cos 2 \theta_{12} \sin^2 \left(\frac{\Delta_{12} L}{2} \right) \cos \beta' - \sin(\Delta_{12} L) \sin \beta' \right],
\end{aligned} \tag{7}$$

where $A_{\nu_e}(R_\odot)$ and $A_{\nu_x}(R_\odot)$ are, respectively, the probability amplitudes of the neutrino to be found in the state ν_e and ν_x ($x = \mu, \tau$) at the solar surface and $\beta' \equiv \text{Arg}[A_{\nu_e}(R_\odot) A_{\nu_x}^*(R_\odot)]$, is the phase difference developed in the flavor basis corresponding to the one we have in Eq. (6) between the mass eigenstates, namely, β . We note that the following relation holds:

$$\begin{aligned}
|A_{\nu_e}(R_\odot)|^2 &= \cos^2 \theta_{12} |A_{\nu_1}(R_\odot)|^2 + \sin^2 \theta_{12} |A_{\nu_2}(R_\odot)|^2 \\
&\quad + \sin 2 \theta_{12} |A_{\nu_1}(R_\odot) A_{\nu_2}(R_\odot)| \cos \beta.
\end{aligned} \tag{8}$$

In this work, we first compute the values of $A_{\nu_e}(R_\odot)$ and $A_{\nu_x}(R_\odot)$ by numerically integrating the neutrino evolution equation in Eq. (1) with the solar electron density taken from Ref. [43] and then compute the final probability at the Earth by using the expression in Eq. (7). We take into account the effect due to the eccentricity of the Earth orbit around the Sun by taking the time average over one year of the probability using the time dependent distance $L(t)$,

$$L(t) = L_0 \left[1 - \epsilon \cos \left(2\pi \frac{t}{T} \right) \right] + \mathcal{O}(\epsilon^2), \tag{9}$$

where $L_0 = 1$ AU, $\epsilon = 0.0167$ is the orbit eccentricity and $T =$ one year. We neglect the correction terms of $\mathcal{O}(\epsilon^2)$.

Following Ref. [41], we restrict the range of Δm^2 from 10^{-11} to 10^{-8} eV². One can easily estimate from Eqs. (3) and (4), that for the typical energy of ⁸B neutrinos, ~ 10 MeV, in order to have appreciable oscillation effects for solar neutrinos, the Δm_{12}^2 value must be larger than of the order $\sim 10^{-11}$ eV². This sets our lower limit on Δm_{12}^2 .

It is known (see, e.g., Ref. [41]) that if Δm_{12}^2 is larger than $\sim 10^{-8}$ eV², the final ν_e survival probability at the Earth, averaged over the neutrino energy, would not practically depend on the precise value of the Sun-Earth distance since the variation in the probability due to the energy spread is large enough, even for ⁷Be neutrinos, to average out the vacuum oscillation effect. Since we do not regard such a case as a LVO solution, this sets our upper limit on Δm_{12}^2 . Also, to cover values of Δm_{12}^2 up to 10^{-8} eV² means to examine the effect of the solar matter on the LVO solution to the SNP whose relevance was already discussed in Refs. [40,41].

B. Three flavor case

For the case when we consider three flavor mixing, the evolution equation of neutrinos in matter can be written as

$$i \frac{d}{dx} \begin{bmatrix} \nu_e \\ \nu_\mu \\ \nu_\tau \end{bmatrix} = \left\{ \begin{bmatrix} V_e(x) & 0 & 0 \\ 0 & 0 & 0 \\ 0 & 0 & 0 \end{bmatrix} + U \begin{bmatrix} 0 & 0 & 0 \\ 0 & \Delta_{12} & 0 \\ 0 & 0 & \Delta_{13} \end{bmatrix} U^\dagger \right\} \times \begin{bmatrix} \nu_e \\ \nu_\mu \\ \nu_\tau \end{bmatrix}, \quad (10)$$

where $\Delta_{ij} \equiv \Delta m_{ij}^2 / 2E$ and we take the representation of the Maki-Nakagawa-Sakata [12] mixing matrix U which is the leptonic analogue of the Cabibbo-Kobayashi-Maskawa matrix in the quark sector [44] as,

$$U = e^{i\lambda_7 \theta_{23}} e^{i\lambda_5 \theta_{13}} e^{i\lambda_2 \theta_{12}}. \quad (11)$$

Explicitly,³

$$U = \begin{bmatrix} c_{12}c_{13} & s_{12}c_{13} & s_{13} \\ -s_{12}c_{23} - c_{12}s_{23}s_{13} & c_{12}c_{23} - s_{12}s_{23}s_{13} & s_{23}c_{13} \\ s_{12}s_{23} - c_{12}c_{23}s_{13} & -c_{12}s_{23} - s_{12}c_{23}s_{13} & c_{23}c_{13} \end{bmatrix}, \quad (12)$$

where λ_i are the SU(3) Gell-Mann's matrices and $c_{ij} = \cos \theta_{ij}$, $s_{ij} = \sin \theta_{ij}$. We assume Δm_{13}^2 to be in the range $\sim 10^{-3} - 10^{-2}$ eV², which is consistent with atmospheric neutrino observations [23]. Because of this assumption, the relation $V_e, \Delta_{12} \ll \Delta_{23} \sim \Delta_{13}$ holds.

In this case, Δ_{13} is the dominant term in the Hamiltonian matrix and this leads to the decoupling of ν_3 from the remaining two states. This means that the oscillation which is driven by the Δ_{13} term can be simply averaged out in the final survival probability of electron neutrinos at the Earth, $P_{3g}(\nu_e \rightarrow \nu_e)$, yielding the relation [29,30]

$$P_{3g}(\nu_e \rightarrow \nu_e) = \sin^4 \theta_{13} + \cos^4 \theta_{13} \cdot P_{2g}(\tilde{\nu}_e \rightarrow \tilde{\nu}_e), \quad (13)$$

where $P_{2g}(\tilde{\nu}_e \rightarrow \tilde{\nu}_e)$ is defined as the survival probability of the following effective two generation system [29,31,30]:

$$i \frac{d}{dx} \begin{bmatrix} \tilde{\nu}_e \\ \tilde{\nu}_\mu \end{bmatrix} = \begin{bmatrix} \cos^2 \theta_{13} \cdot V_e(x) & \frac{1}{2} \Delta_{12} \sin 2\theta_{12} \\ \frac{1}{2} \Delta_{12} \sin 2\theta_{12} & \Delta_{12} \cos 2\theta_{12} \end{bmatrix} \begin{bmatrix} \tilde{\nu}_e \\ \tilde{\nu}_\mu \end{bmatrix}, \quad (14)$$

where $\tilde{\nu}_\alpha$ ($\alpha = e, \mu, \tau$) is defined as

$$\begin{bmatrix} \tilde{\nu}_e \\ \tilde{\nu}_\mu \\ \tilde{\nu}_\tau \end{bmatrix} = e^{-i\lambda_5 \theta_{13}} e^{-i\lambda_7 \theta_{23}} \begin{bmatrix} \nu_e \\ \nu_\mu \\ \nu_\tau \end{bmatrix}. \quad (15)$$

We compute $P_{2g}(\tilde{\nu}_e \rightarrow \tilde{\nu}_e)$ by using the expression in Eq. (7) just by replacing the solar electron density as $N_e(r) \rightarrow \cos^2 \theta_{13} \cdot N_e(r)$.

We note that we have three independent parameters Δm_{12}^2 , θ_{12} , and θ_{13} which can be fitted or constrained by the experimental data. Regarding θ_{13} , it is clear that the probability in Eq. (13) is invariant under $\theta_{13} \rightarrow \pi - \theta_{13}$ allowing us to restrict the range of θ_{13} to $0 \leq \theta_{13} \leq \pi/2$. As for Δm_{12}^2 and θ_{12} , we again consider the range given in Eq. (5) for the case of two generations, since the same argument discussed in the previous subsection also holds for $P_{2g}(\tilde{\nu}_e \rightarrow \tilde{\nu}_e)$.

III. DATA ANALYSIS

The general idea is to perform a χ^2 analysis to fit the oscillation free parameters (θ_{12} and Δm_{12}^2 , in the case of two generations, and θ_{12} , θ_{13} , and Δm_{12}^2 in the case of three generations) with observed experimental data. We investigate in addition the effect of having an extra normalization factor f_B for the ⁸B neutrino flux, which is in this case assumed to be free. In what follows we will give explicit definitions of the χ^2 for the solar rates, the SK recoil-electron spectrum, the SK zenith angle distribution, as well as the combination of both, to be used in our analysis.

A. Calculation of the rates

We calculate, for the two (three) generation framework, our theoretical predictions for the measured solar neutrino rates as a function of the two (three) mixing parameters for the gallium and chlorine experiments by folding the neutrino oscillation probability P_{2g} (P_{3g}) with interaction cross section and the six solar neutrino fluxes corresponding to each

³Here we neglect the possible CP violating phase since this phase will not affect the ν_e survival probability, even if we take into account the next-to-leading order corrections in electroweak interactions [45].

reaction pp , pep , ${}^7\text{Be}$, ${}^8\text{B}$, ${}^{13}\text{N}$, and ${}^{15}\text{O}$ as predicted by the standard solar model of Bahcall and Pinsonneault [8] (BP98 SSM). Other minor sources such as ${}^{17}\text{F}$ and hep are not considered for simplicity. For gallium and chlorine experiments, we use the neutrino absorption cross sections found in Ref. [43] and for the SK experiment, we use the new calculation of ν_e, ν_μ, ν_τ scattering cross section on electrons which take into account radiative corrections [46].

In this case the expected event rate for Ga and Cl detectors that should be compared to experimental data is

$$R_x^{\text{theo}} = C_x \int dE \sigma_x(E) \langle P_n(E) \rangle \times \left(f_B \phi_B(E) + f_{\text{Be}} \phi_{\text{Be}}(E) + \sum_j \phi_j(E) \right), \quad (16)$$

where $x = \text{Ga, Cl}$, $n = 2g, 3g$, $\phi_B(E)$, $\phi_{\text{Be}}(E)$, and $\phi_j(E)$ with $j = pp, pep, {}^{13}\text{N}$, and ${}^{15}\text{O}$ are the neutrino fluxes as a function of the neutrino energy taken from Ref. [8], and C_x is some normalization constant determined in such a way that R_x^{theo} is given in solar neutrino unit (SNU). The numbers f_B and f_{Be} are, respectively, the normalization constants for

the ${}^8\text{B}$ and the ${}^7\text{Be}$ neutrino fluxes, $f_B = f_{\text{Be}} = 1$ corresponds to the BP98 SSM values. Here $\langle P_n \rangle$ means that the probability has been averaged on the neutrino path length to take into account the eccentricity of the Earth orbit around the Sun, after we have computed the probability as in Eq. (7), for two generations, or as in Eq. (13), for three generations, with the solar matter effect included. The integral above was performed starting at the energy threshold of each experiment.

In our calculations, we have also included the effect due to the thermal broadening of about 1 keV of the ${}^7\text{Be}$ lines [47] when computing the capture rate by performing an extra average over the two ${}^7\text{Be}$ neutrino energy profiles given in Ref. [47]. This is pertinent for large values of Δm_{12}^2 as discussed, e.g., in Refs. [48,41].

When f_B is taken to be free we assume the power-law relationship between the ${}^8\text{B}$ and ${}^7\text{Be}$ fluxes, given by $\phi^{7\text{Be}} = (\phi^{8\text{B}})^{10/24}$ [37], in order to renormalize the ${}^7\text{Be}$ flux by a factor f_{Be} as

$$f_{\text{Be}} = f_B^{10/24}. \quad (17)$$

For the SK experiment, the expected solar neutrino event rate, normalized by the BP98 SSM prediction, is given by

$$R_{\text{SK}}^{\text{theo}} = \frac{f_B \int dE_e \int dE'_e h(E'_e, E_e) \int dE_\nu \phi_B(E_\nu) \left(\frac{d\sigma_{\nu_e}}{dE'_e} \langle P_n(E_\nu) \rangle + \frac{d\sigma_{\nu_x}}{dE'_e} [1 - \langle P_n(E_\nu) \rangle] \right)}{\int dE_e \int dE'_e h(E'_e, E_e) \int dE_\nu \phi_B(E_\nu) \frac{d\sigma_{\nu_e}}{dE'_e}}, \quad (18)$$

where E_e is the observed recoil electron energy, E'_e is the true recoil electron energy, $h(E'_e, E_e)$ is the electron energy resolution function taken from Ref. [49], and $d\sigma_{\nu_e}/dE'_e$, $d\sigma_{\nu_x}/dE'_e$ are $\nu_e - e$ and $\nu_x - e$ ($x = \mu, \tau$) scattering cross sections taken from Ref. [46]. In the integral above we have used 5.5 MeV as the energy threshold for SK.

The definition of the χ_{rates}^2 function to be minimized is the same as the one used in Ref. [50] which essentially follows the prescription given in Ref. [51]. Explicitly,

$$\chi_{\text{rates}}^2 = \sum_{x,y} (R_x^{\text{theo}} - R_x^{\text{obs}}) \sigma_{xy}^{-2} (R_y^{\text{theo}} - R_y^{\text{obs}}), \quad (19)$$

where $x(y)$ runs through four solar neutrino experiments, Homestake, SAGE, GALLEX/GNO combined, and Super-Kamiokande, the theoretical predictions $R_{x(y)}^{\text{theo}}$ are given in Eqs. (16) and (18) and the experimental values $R_{x(y)}^{\text{obs}}$ are given in Table I. The error matrix σ_{xy} contains the theoretical and experimental uncertainties according to Ref. [50] where theoretical uncertainties are taken from the ones given by the BP98 SSM [8].

B. Calculation of the SK recoil-electron spectrum

For the spectrum shape analysis we first define the following quantity:

$$S_i^{\text{theo}} \equiv \frac{\int_{E_i^{\text{min}}}^{E_i^{\text{max}}} dE_e \int dE'_e h(E'_e, E_e) \int dE_\nu \phi_B(E_\nu) \left(\frac{d\sigma_{\nu_e}}{dE'_e} \langle P_n(E_\nu) \rangle + \frac{d\sigma_{\nu_x}}{dE'_e} [1 - \langle P_n(E_\nu) \rangle] \right)}{\int_{E_i^{\text{min}}}^{E_i^{\text{max}}} dE_e \int dE'_e h(E'_e, E_e) \int dE_\nu \phi_B(E_\nu) \frac{d\sigma_{\nu_e}}{dE'_e}}, \quad (20)$$

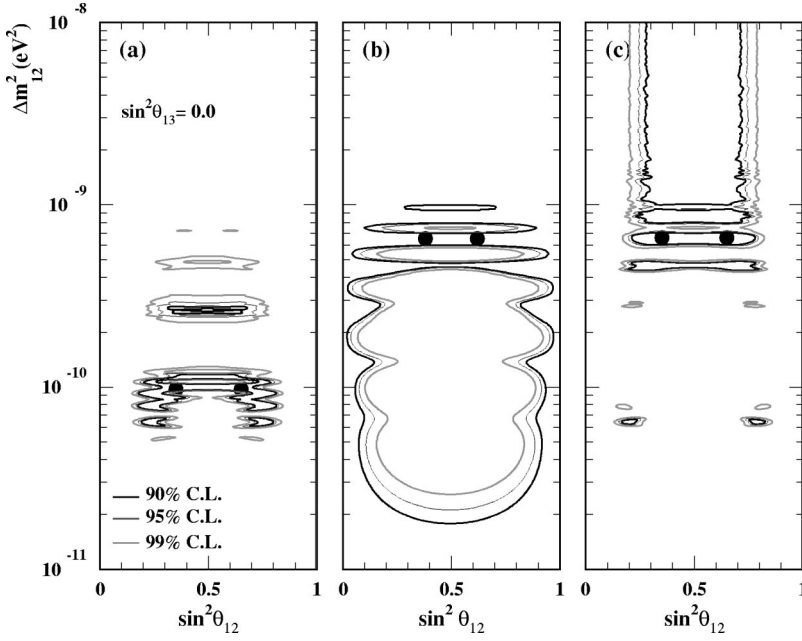


FIG. 2. Region of $(\sin^2 \theta_{12}, \Delta m_{12}^2)$ allowed by (a) the total rates from ^{37}Cl , ^{71}Ga , and SK experiments, (b) the SK spectrum, and (c) the combined analysis of rates + SK spectrum in the long-wavelength vacuum oscillation scenario for two neutrino flavors. In the case of the SK spectrum (b) it is the inner part of the contours which is excluded by the data. The best fit points are shown as black circles. Solar matter effect is not taken into account.

where E_i^{\min} and E_i^{\max} are the minimum and maximum observed recoil electron energy in the i th bin, starting at the 5.5 MeV threshold for the SK detector. In total we have 18 bins taken at 0.5 MeV intervals, except for the last bin which includes all the contribution above 14 MeV.

The definition of the χ_{spec}^2 function to be minimized is the same as the one used in Ref. [17], that is,

$$\chi_{\text{spec}}^2 = \sum_{i,j=1,18} (\alpha S_i^{\text{theo}} - S_i^{\text{SK}}) \sigma_{ij}^{-2} (\alpha S_j^{\text{theo}} - S_j^{\text{SK}}), \quad (21)$$

where σ_{ij} were computed as prescribed in Ref. [17] and S_i^{SK} are the experimental points whose numerical values are graphically reproduced from Ref. [6]. We will not use the new 5 MeV point since the systematic errors of this point are still under study by the SK Collaboration. The extra normalization parameter α , which is always taken to be free in our

analysis, is introduced because here we are only interested in fitting the shape of the spectrum. Moreover when we combine with the rates, it allows us to avoid double counting the information already taken into account in the rate analysis.

For the SK spectrum analysis, as a good approximation, we simply assume that neutrinos exit from the Sun as pure ν_e and use the vacuum probability formula in Eq. (3), for two generation, or in Eq. (13), for three generation, in this latter case removing from our expression the Sun matter effect. This is well justified by the discussion we presented in Sec. II A.

C. Calculation of the zenith angle dependence

We define the χ_{zenith}^2 , for the zenith angle dependence, as follows:

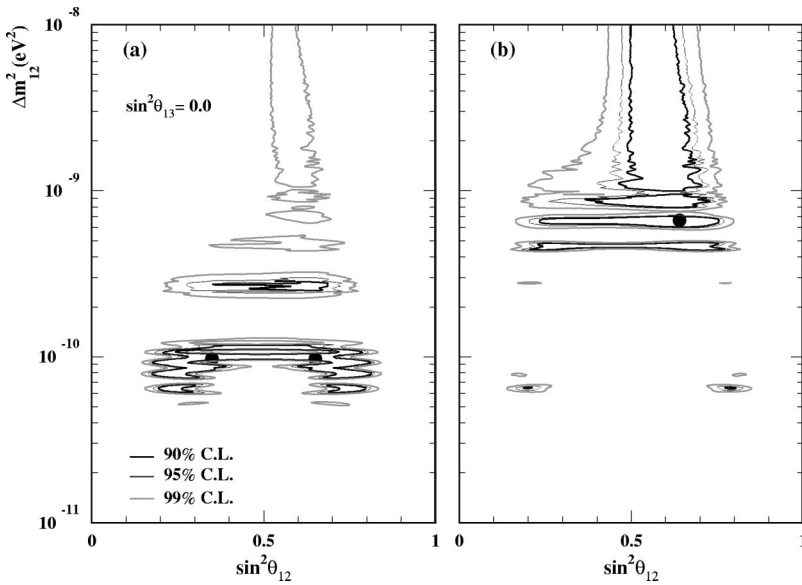


FIG. 3. Same as in Figs. 2(a) and 2(c) but with the solar matter effect.

TABLE II. The best fitted parameters and χ^2_{\min} as well as C.L. (in %) for the two generation LVO solution to the SNP. The number of degrees of freedom (N_{DOF}) are also indicated. The matter effect was taken into account unless it is indicated in parentheses. Note that for spectrum analysis matter effect was neglected, as it is a good approximation (see Secs. II A, III B). We also present the values of the local best fit which explain better the total rates in the line indicated as combined (R).

Case	$\Delta m_{12}^2 \times 10^{10} \text{ eV}^2$	$\sin^2 \theta_{12}$	f_B	χ^2_{\min}	N_{DOF}	C.L. (%)
Rates	0.97	0.35/0.65	1 (fixed)	0.25	2	88.2
Spectrum	6.5	0.38/0.62		10.5	15	78.7
Combined (w/o matter)	6.6	0.35/0.65	1 (fixed)	25.1	24	40.0
Combined	6.6	0.64	1 (fixed)	23.9	24	46.7
Combined (R)	0.65	0.2/0.8	1 (fixed)	28.0	24	26.0
Rates	0.88	0.34/0.66	1.21	0.01	1	91.6
Combined (w/o matter)	6.6	0.31/0.69	0.72	22.7	23	47.8
Combined	6.6	0.66	0.74	21.7	23	53.8
Combined (R)	0.65	0.2/0.8	0.86	27.5	23	23.5

$$\chi^2_{\text{zenith}} = \sum_{i=1,6} \frac{(\beta Z_i^{\text{theo}} - Z_i^{\text{obs}})^2}{\sigma_{Z,i}^2}, \quad (22)$$

where Z_i^{theo} is the i th bin theoretical expectation, Z_i^{obs} is the i th bin observed value, with five night bins and one day bin which are graphically reproduced from Ref. [6] and β is a free normalization constant introduced for the same reasons as in the case of the spectrum analysis. As the LVO solution does not imply in practice any zenith angle distortion of the data, this will simply provide an extra global constant that will increase the final combined χ^2_{\min} . It is important to remark that this global constant will only affect the quality of the combined fit, bearing no influence on the computed allowed region. We obtained $\chi^2_{\text{zenith}} = 4.3$ with $\beta = 0.47$ for the zenith angle distribution.

D. Combined analysis

Finally the combined χ^2 to be minimized is simply defined as the sum of the individual ones

$$\chi^2_{\text{comb}} = \chi^2_{\text{rates}} + \chi^2_{\text{spec}} + \chi^2_{\text{zenith}}. \quad (23)$$

E. Definitions of the confidence levels and N_{DOF}

Using the χ^2 functions defined in the previous subsections, for the two generation analysis where we have only two mixing parameters (Δm_{12}^2 , θ_{12}), we use the condition $\chi^2 = \chi^2_{\min} + \Delta\chi^2$ where $\Delta\chi^2 = 4.61, 5.99$, and 9.21 for 90, 95, and 99 % C.L., respectively, in order to determine the allowed parameter space. On the other hand, for the three generation analysis, in order to constrain the parameter space spanned by three variables (Δm_{12}^2 , θ_{12} , θ_{13}), we determine the isoconfidence level surface by the condition $\chi^2 = \chi^2_{\min} + \Delta\chi^2$ where $\Delta\chi^2 = 6.25, 7.82$, and 11.36 for 90, 95, and 99 % C.L., respectively, as in Ref. [35].

We note that in this work, we always determine the values of χ^2_{\min} within the range $10^{-11} \text{ eV}^2 < \Delta m_{12}^2 < 10^{-8} \text{ eV}^2$ and

therefore, do not take into consideration the region relevant for MSW solutions [16,17]. This means that in this work, we assume *a priori* that LVO is the solution to the solar neutrino problem, so adopting a different criteria than other authors, see, e.g., Ref. [36], to draw the C.L. contours.

Here, we also describe how we compute the number of degrees of freedom N_{DOF} which is relevant to determine the goodness of fit (or C.L.). We compute N_{DOF} as follows:

$$N_{\text{DOF}} \equiv N_{\text{data}} - N_{\text{param}} - N_{\text{norm}}, \quad (24)$$

where N_{data} is the number of the data points we use in each analysis, N_{param} is the number of mixing parameters to be constrained, two or three depending on the number of neutrino generations considered, and N_{norm} is the number of extra free normalization factors we introduced in the analysis, i.e., f_B in Eqs. (16) and (18), α in Eq. (21) and β in Eq. (22).

IV. RESULTS WITH THE TWO GENERATION SCHEME

In this section we discuss our results for the analysis of the solar neutrino data in the context of two generations.

A. Results with fixed f_B

We first present the case when we fix $f_B = 1$, therefore $f_{\text{Be}} = 1$. This corresponds to use the BP98 SSM flux values. To demonstrate the influence of the solar matter in the computed allowed regions, we will show here our results without and with the MSW effect in the Sun.

In Figs. 2(a), 2(b), and 2(c) we show the allowed region in $\sin^2 \theta_{12} - \Delta m_{12}^2$ parameter space, for the rates, spectrum and combined analysis, respectively, without taking into account any possible influence of the solar matter, hence all the plots are symmetric with respect to $\sin^2 \theta_{12} = 0.5$ because of the invariance of the pure vacuum probability under the transformation $\theta_{12} \rightarrow \pi/2 - \theta_{12}$.

In Figs. 3(a) and 3(b) we show the allowed region in $\sin^2 \theta_{12} - \Delta m_{12}^2$ parameter space, for the rates and combined

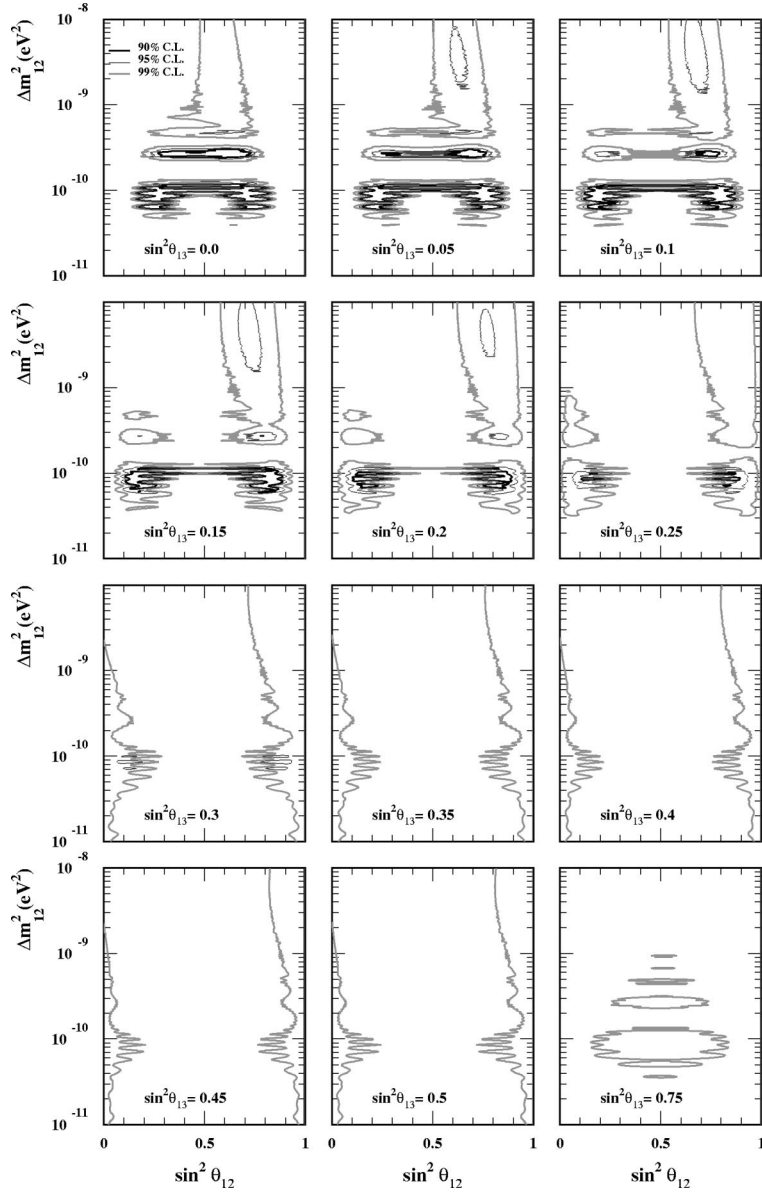


FIG. 4. Region of $(\sin^2 \theta_{12}, \Delta m_{12}^2)$ allowed by the total rates from ^{37}Cl , ^{71}Ga , and SK for various values of $\sin^2 \theta_{13}$ for the long-wavelength vacuum oscillation solution to the SNP with three neutrino flavors.

analysis, respectively, taking into account the MSW effect. As expected we see that in this case the shape of the allowed region is not symmetric with respect to $\sin^2 \theta_{12} = 0.5$, for $\Delta m_{12}^2 \geq 3 \times 10^{-10} \text{ eV}^2$, in good agreement with the results obtained in Ref. [41]. We also observe that there is a region allowed at 99 % C.L. for $\Delta m_{12}^2 > 4 \times 10^{-10} \text{ eV}^2$ that only appears when matter effects are taken into account.

No spectrum analysis with the solar matter effect was performed since we have checked that the results are essentially the same as the one presented in Fig. 2(b). This is because of the fact that nearly all neutrinos that are relevant to SK exit from the Sun as pure ν_e and so we can simply use the vacuum oscillation formulas as a very good approximation (see the discussions in Sec. II A).

The values of the χ_{\min}^2 , the best fitted parameters, the number of degrees of freedom (N_{DOF}), as well as the goodness of the fit, the C.L. in %, for the above discussed situations are shown in Table II. In this table we also include this information for the local best fit point we found at Δm^2

$= 6.5 \times 10^{-11} \text{ eV}^2$ and $\sin^2 2\theta_{12} = 0.2/0.8$ which explain somewhat better the rates than the global best fit one.

The MSW effect does not affect the values of the best fitted parameters for the spectrum and rates analysis, given two virtually symmetric solutions in $\sin^2 \theta_{12}$. This symmetry is broken, however, when we combine rates and spectrum. Since the spectrum data prefers larger values of Δm_{12}^2 , the combined best fit point will lay in an allowed island slightly deformed by the matter potential.

Comparing the region allowed by the spectrum at 90 % C.L., given in Fig. 2(b), with the one allowed by the rates at the same C.L., given in Fig. 3(a), we can see that in general the region favored by the total rates are disfavored by the spectrum information. The SK spectrum data shows practically no energy dependent distortion, preferring either larger values of Δm_{12}^2 , where the oscillating term gets averaged to one half, or smaller values of Δm_{12}^2 , where the oscillating term vanishes. The total rates, however, prefer intermediate values of Δm_{12}^2 , where the energy dependence of the solu-

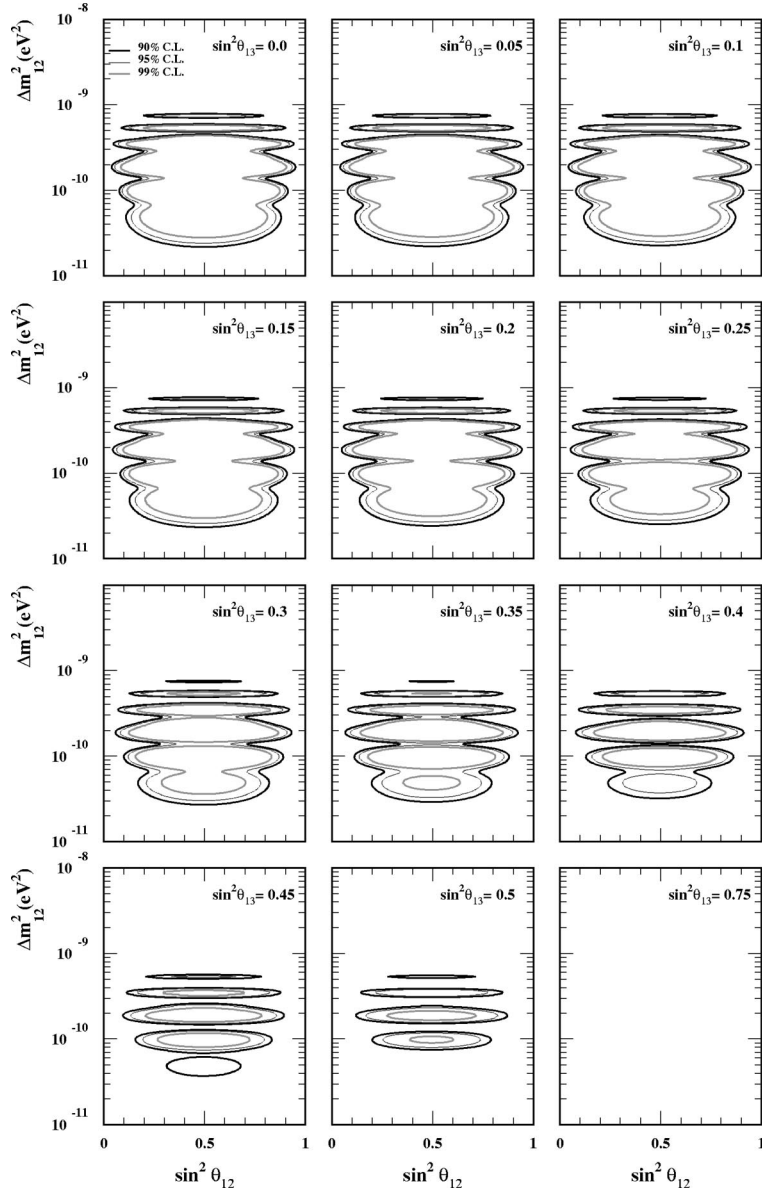


FIG. 5. Region of $(\sin^2 \theta_{12}, \Delta m_{12}^2)$ allowed by the SK spectrum for various values of $\sin^2 \theta_{13}$ for the LVO solution to the SNP with three neutrino flavors. It is the inner part of the contours which is excluded by the data.

tion provides the proper reduction to explain the four data points. Due to such disagreement between the total rates and the SK spectrum, we find it difficult to get a good fit for both at the same time. We note that the combined allowed regions are basically formed by the parameters which are more consistent with the spectrum data.

In spite of this incompatibility we note that the quality of the combined $\chi^2_{\min}/\text{DOF}=23.9/24$ seems to be quite good. This can be understood in virtue of the fact that the oscillation parameters at this minimum can provide a very good explanation for the SK spectrum ($\chi^2_{\min}=10.7$) and zenith angle dependence ($\chi^2_{\min}=4.3$), which are the majority of the statistical points, even though they give a generally poor explanation for the total rates ($\chi^2_{\min}=8.9$). In fact the oscillation parameters at the combined minimum correctly predict the ^{71}Ga rate but for Homestake and SK the predicted values are substantially above what is measured by those experiments.

B. Results with arbitrary f_B

For the case where we consider f_B as a free parameter we also have performed the same analysis without and with matter effect taken into account. Although the allowed regions for the rates and the combined analysis increased a little bit they are substantially the same as the ones shown in Figs. 2 and 3 so we do not show them here.

Again, the values of the χ^2_{\min} as well as of the best fitted parameters can be found in Table II. In comparison to the fixed f_B case, the fit for the rates is substantially improved and the allowed parameter region became somewhat larger. The other qualitative features mentioned in the previous subsection remain unchanged.

The combined fit also improved a bit by this extra freedom given $\chi^2_{\min}/N_{\text{DOF}}=21.7/23$ (see Table II), which seems to be even better than in the previous case. Allowing the ^8B flux to be free does not affect the fit of the SK spectrum and zenith dependence data, but it improves a little the fit for the

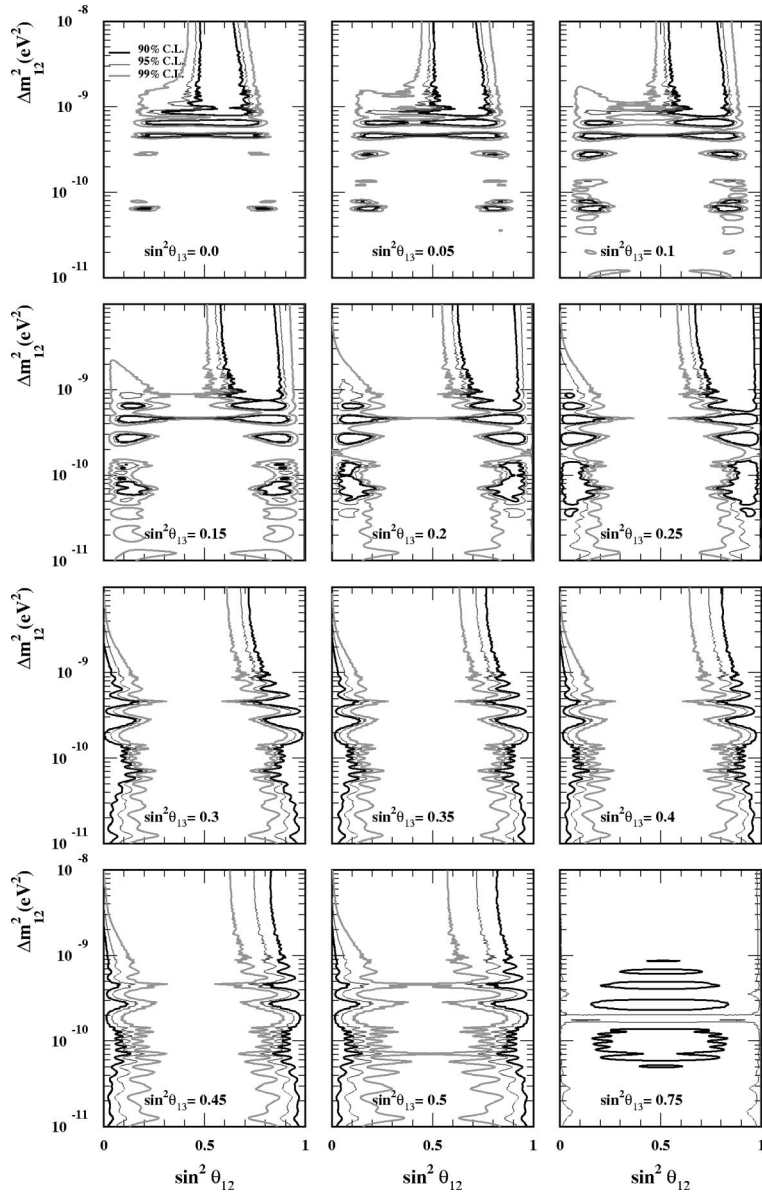


FIG. 6. Same as in Fig. 4 but for the combined analysis of total rates + SK spectrum.

rates ($\chi^2_{\min}=6.7$) since we can now correctly predict the ^{71}Ga and SK rates but still over estimate the Homestake value.

V. RESULTS WITH THE THREE GENERATION SCHEME

In this section we discuss our results for the analysis of the solar neutrino data in the context of three neutrino generations. Here we will always present the results taking into account the solar matter effect.

A. Results with fixed f_B

As for the two generation case we first consider f_B as fixed to be 1. In Fig. 4 we show the regions, in $\sin^2 \theta_{12} - \Delta m^2_{12}$ parameter space, allowed by the rates for different values of $\sin^2 \theta_{13}$. In each plot of Fig. 4 we are presenting a *cut* of the allowed parameter space in three generations, that is, we show the allowed region in the $\sin^2 \theta_{12} - \Delta m^2_{12}$ plane

for a given value of $\sin^2 \theta_{13}$, which means that the χ^2_{\min} value is common for all the plots shown. We found that for the rates the best fit occurs when $\sin^2 \theta_{13}=0$.

We note that, as in the case of the two generation analysis, the allowed regions that appear in the plots are asymmetric for $\Delta m^2_{12} \gtrsim 3 \times 10^{-10} \text{ eV}^2$ because of the matter effect in the Sun. Moreover, there is a tendency that the matter influence will gradually start to be important at smaller values of Δm^2_{12} as $\sin^2 \theta_{13}$ increases. We can understand this by recalling that the effective potential here has been rescaled by $\cos^2 \theta_{13}$ [see Eq. (14)], which means that as $\sin^2 \theta_{13}$ increases, the potential decreases and can start to be relatively relevant for lower values of Δm^2_{12} .

In Fig. 5 the regions, in $\sin^2 \theta_{12} - \Delta m^2_{12}$ parameter space, allowed by the spectrum for different values of $\sin^2 \theta_{13}$ are displayed. Since we have used the vacuum oscillation formulas in our spectrum calculation, the allowed regions are symmetric with respect to $\sin^2 \theta_{12}=0.5$. Again, as in the case of

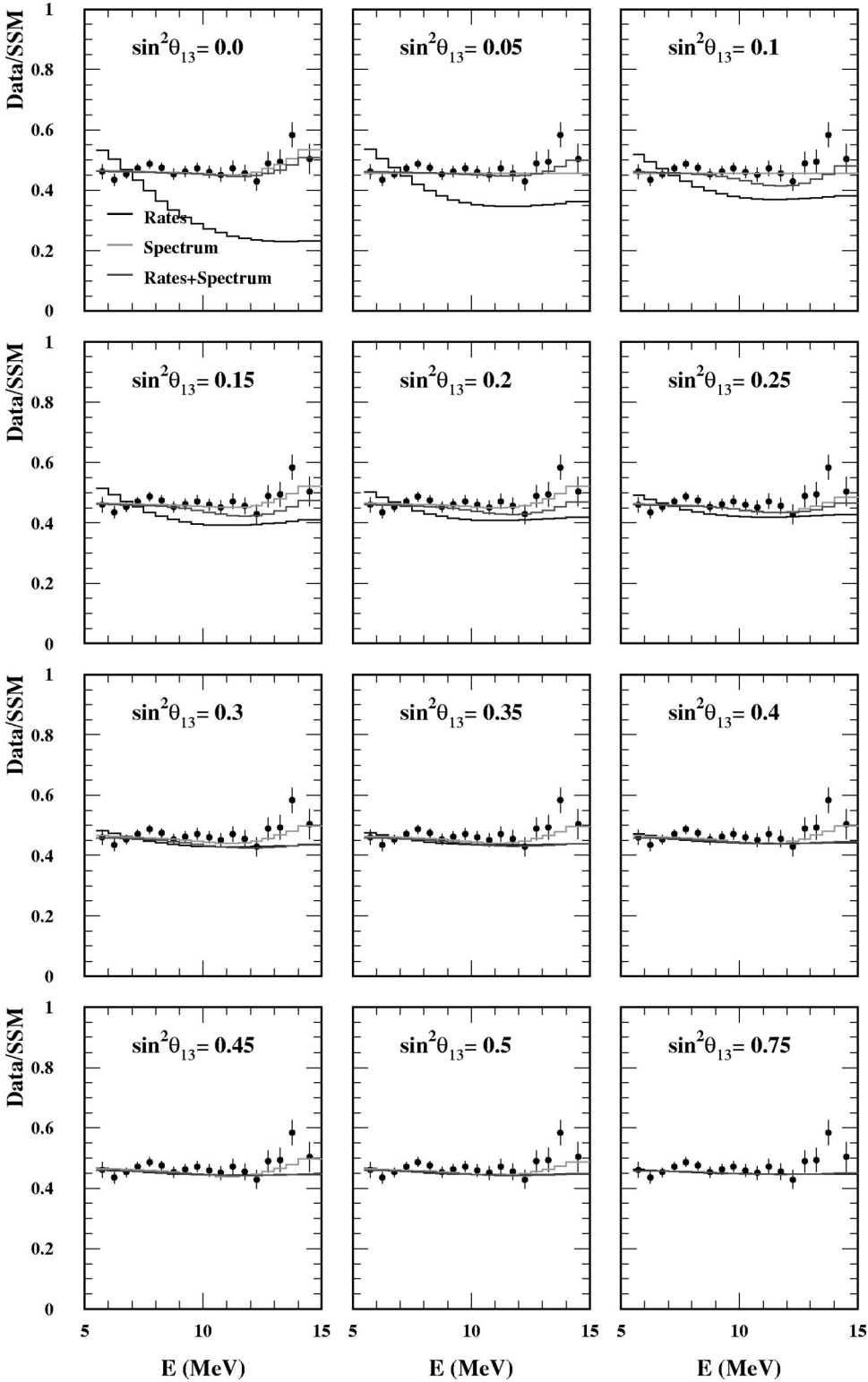


FIG. 7. Expected SK spectrum using the best fitted values of $(\sin^2 \theta_{12}, \Delta m_{12}^2)$. We note that the spectrum curves determined only by the rates are adjusted in such a way that χ^2 defined in Eq. (21) takes minimum values after we determine the values of $(\sin^2 \theta_{12}, \Delta m_{12}^2)$ by the fit only with the rates.

the rates analysis, we found the best fit at $\sin^2 \theta_{13}=0$. We note that although the best fit occurs when $\theta_{13}=0$, the region excluded by the spectrum data become smaller as θ_{13} increases. This can be qualitatively understood from the fact that the energy dependence of the probability becomes weaker as θ_{13} increases [see Eq. (13)] and consequently, the spectrum become flatter, which is consistent with the present SK data.

In Fig. 6 we plot the combined allowed region for rates and spectrum, for fixed $f_B=1$. The values we have obtained for the best fitted parameters and χ^2_{\min} as well as the estimated C.L. of the fit are presented in Table II. We have found that for the combined analysis, the best fit occurs when $\sin^2 \theta_{13}=0.12$. Notwithstanding, a small difference in χ^2 such as $\chi^2_{\min}(\theta_{13}=0) - \chi^2_{\min}(\theta_{13}=0.12) \approx 0.6$ clearly bears no real statistical significance to the preferred nonzero θ_{13} .

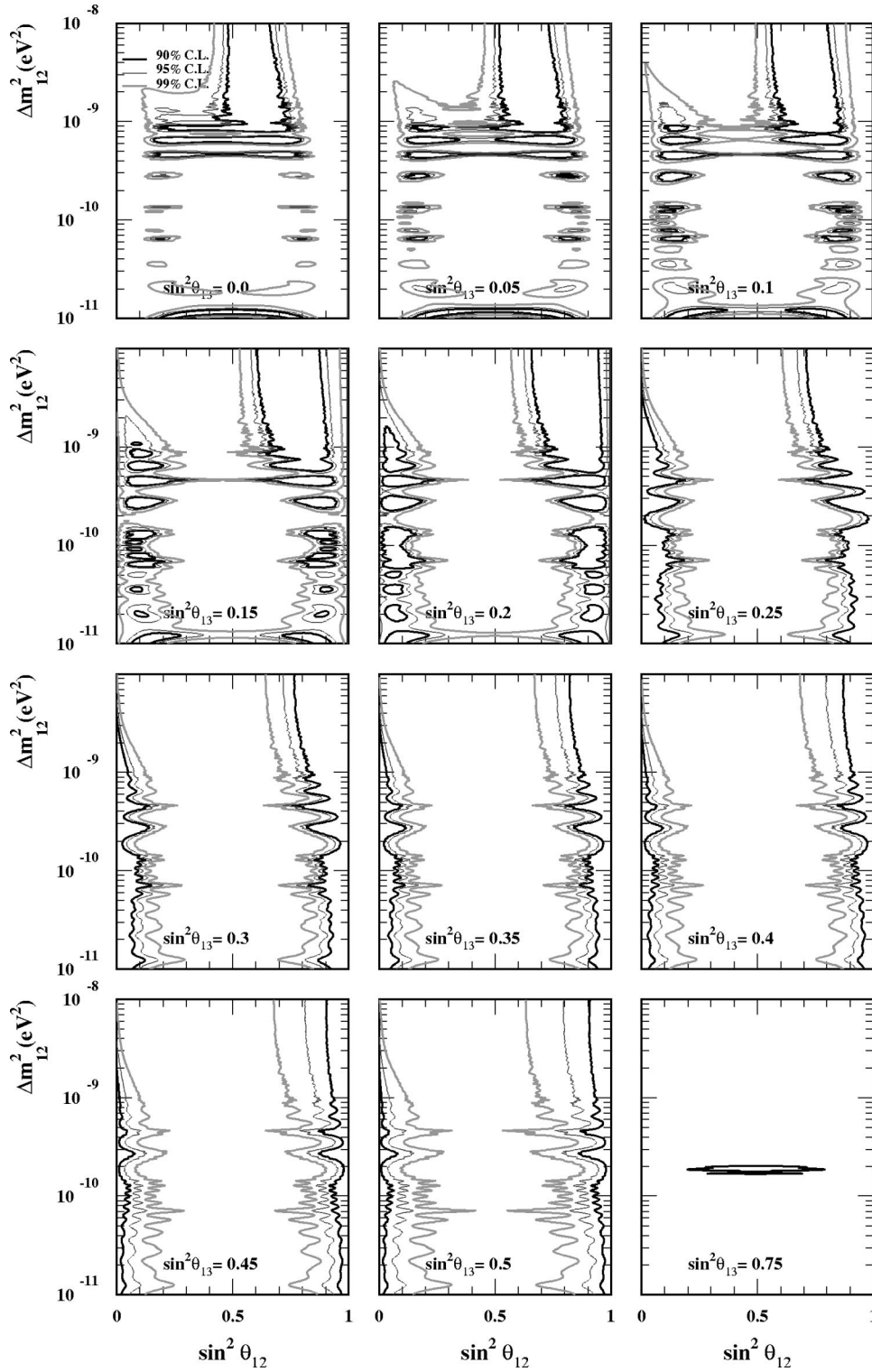


FIG. 8. Same as in Fig. 6 but with arbitrary ${}^8\text{B}$ neutrino flux normalization f_B .

Finally we plot in Fig. 7 the spectrum calculated for the best fitted parameters for the rates, spectrum and combined analysis, for fixed values of $\sin^2 \theta_{13}$, as well as the SK experimental data points. Here some comments are in order. One of the features of the total rate analysis is that several ‘‘local’’ best fit points, which are rather comparable in terms of χ^2 values, exist. For $\theta_{13}=0$ we found the best fit at $(\Delta m_{12}^2, \sin^2 \theta_{12}) = (9.7 \times 10^{-11} \text{ eV}^2, 0.35/0.65)$. We have

noticed that as we increase the value of θ_{13} these points do not always remain as best fit points but always remain as local best. Moreover, such two symmetric (with respect to $\theta_{12}=45^\circ$) best fit points move smoothly toward the direction of $\theta_{12}=0$ and $\theta_{12}=90^\circ$. The fitted spectrum curves for the rates, shown in Fig. 7, are, strictly speaking, indicating the ‘‘evolution’’ of the spectrum shape of these ‘‘best fit points’’ as θ_{13} increases. We see that the best fit parameters for the

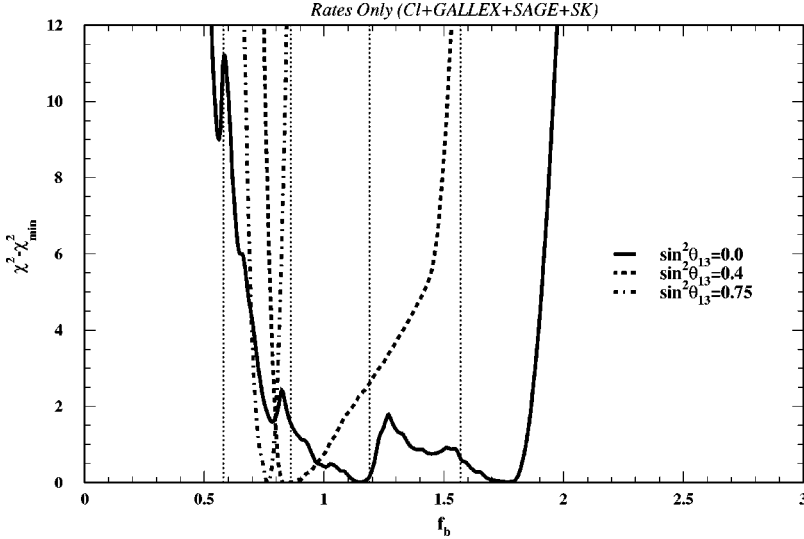


FIG. 9. $\chi^2 - \chi_{\min}^2$ is plotted as a function of f_B for various values of $\sin^2 \theta_{13}$. We also show, by the vertical lines, the range of allowed values of f_B at one and three standard deviations as predicted by the BP98 SSM [8].

rates do not produce a spectrum shape which is consistent with the SK data for lower values of $\sin^2 \theta_{13}$, but the combined fit, which is dominated by the spectrum weight in the χ^2 is in fairly good agreement with the data.

As in the two generation case in spite of the incompatibility between rates and spectrum the quality of the combined fit where we found $\chi_{\min}^2/N_{\text{DOF}}=23.3/23$ is quite good. Here again the oscillation parameters at the minimum can provide a very good explanation for the SK spectrum ($\chi_{\min}^2=11.1$) and zenith angle dependence ($\chi_{\min}^2=4.3$), the majority of the statistical points, even though they give a generally poor explanation for the total rates ($\chi_{\min}^2=7.9$), predicting total rates that are consistent with ^{71}Ga but inconsistent with Homestake and SK data.

B. Results with arbitrary f_B

The same plot as in Fig. 6 is presented for the combined analysis in Fig. 8, when we considered f_B to be free. We do not show the rates or the spectrum allowed regions in this case, since they are virtually the same as the ones shown in Figs. 4 and 5, respectively.

We plot in Fig. 9, $\chi^2 - \chi_{\min}^2$ for the rates as a function of f_B for three values of θ_{13} . From this plot, we can see that as θ_{13} becomes larger the allowed values of f_B become more restricted, eventually, narrower than the range allowed by the BP98 SSM, $0.58 < f_B < 1.57$ at 3σ [8]. The calculated spec-

trum for the best fitted parameters for the rates, spectrum and combined analysis, for various values of $\sin^2 \theta_{13}$, are similar to the case with $f_B=1$, except that the best fit point for the total rates can predict a less distorted spectrum shape at lower values of $\sin^2 \theta_{13}$ than in the previous case. We find it unnecessary to show this here.

The combined fit improved a little with respect to the previous case given $\chi_{\min}^2/N_{\text{DOF}}=21.7/22$. Again allowing the ^8B flux to be free does not affect the fit of the SK spectrum and zenith dependence data, but it improves slightly the fit for the rates.

C. Constraining θ_{13}

The values of the χ_{\min}^2 as well as of the best fitted parameters for all the above cases are shown in Table III. The combined χ^2 value includes χ_{zenith}^2 as for the two generation case. To illustrate the effect of the presence of the third neutrino in the χ^2 , we plot in Fig. 10 the values of $\Delta\chi^2 \equiv \chi^2 - \chi_{\min}^2$ as a function of $\sin^2 \theta_{13}$ for the cases with f_B fixed. From these plots, we see that there is a general tendency that the fit become worse as θ_{13} increases, although we note that there is a local minimum for the fit with the rates and the combined data at $\sin^2 \theta_{13} \sim 0.67$. We also see that $\Delta\chi^2$ for the rates increases more rapidly than that for the spectrum, which rises in fact quite smoothly. This can be understood as follows.

TABLE III. The best fitted parameters and χ_{\min}^2 for the three generation LVO solution to the SNP.

Case	$\sin^2 \theta_{13}$	$\Delta m_{12}^2 \times 10^{10} \text{ eV}^2$	$\sin^2 \theta_{12}$	f_B	χ_{\min}^2	N_{DOF}	C.L. (%)
Rates	0.0	0.97	0.35/0.65	1 (fixed)	0.25	1	61.7
Spectrum	0.0	6.5	0.38/0.62		10.5	14	72.5
Combined	0.12	4.6	0.75	1 (fixed)	23.3	23	44.3
Combined (R)	0.14	0.66	0.15/0.85	1 (fixed)	26.1	23	29.6
Rates	0.0	0.88	0.34/0.66	1.21	0.01	0	–
Combined	0.0	6.6	0.66	0.74	21.7	22	47.7
Combined (R)	0.1	0.65	0.14/0.86	0.82	25.5	22	27.4

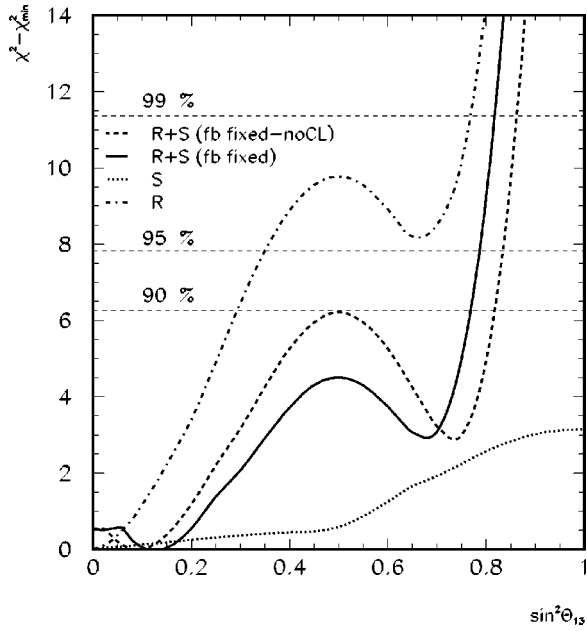


FIG. 10. $\chi^2 - \chi_{\min}^2$ as a function of $\sin^2 \theta_{13}$, for the case when f_B is fixed to be equal to 1 for the rates (R), spectrum (S), combined analysis ($R+S$) and for the combined analysis without ^{37}Cl data ($R+S$ noCL).

As pointed out in Ref. [33], naively, the fit for the rates is expected to become worse as θ_{13} increases since any energy dependence in the probability will become weaker [see Eq. (13)] and thus, in general, the larger the value of θ_{13} , the similar will become the suppressions for all the solar neutrinos, leading to a gradually stronger inconsistency with the observed total rates. On the other hand, as we already mentioned in Sec. V A, the loss of energy dependence will not compromise so much the fit for the spectrum data since the observed spectrum shape is consistent with a flat one.

Finally, from Fig. 10, we can conclude that the solar neutrino data alone give the upper bound $\theta_{13} \lesssim 60^\circ$ at 95 % C.L. It is interesting to observe that this limit is quite similar to the one obtained in the case of a three flavor MSW solution to the SNP [35], although this MSW analysis was performed with different data.

VI. PREDICTIONS FOR SEASONAL VARIATIONS

In this section we discuss, in view of our previous presented results, possible seasonal variations that could be measured by the current Super-Kamiokande detector, as well as by the future Borexino [52] and KamLAND [53] experiments, which will be sensitive to ^7Be neutrinos. It is clear that because of the eccentricity of the Earth orbit around the Sun, solar neutrino fluxes should vary as $1/L^2$ as L varies with time. From Eq. (9) we can estimate that the flux variation in one year due to this effect is

$$\Delta \phi_\nu \sim \Delta \left(\frac{1}{L^2} \right) \sim \frac{4\epsilon L_0}{L^3} \sim 4\epsilon \phi_\nu \sim 0.07 \phi_\nu, \quad (25)$$

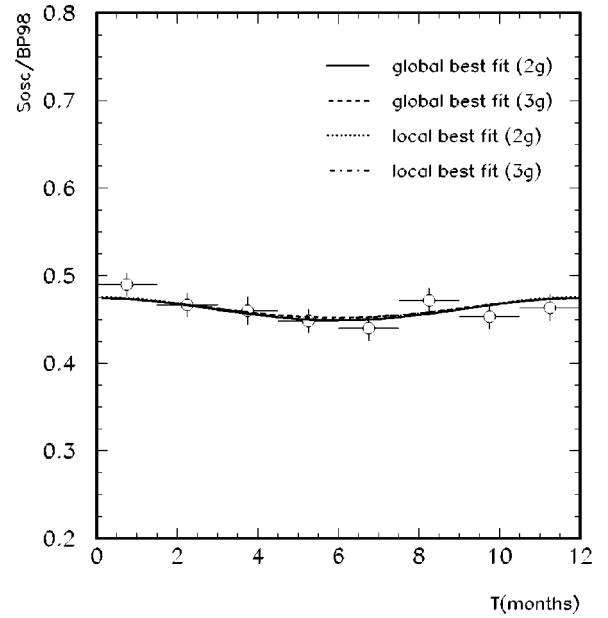


FIG. 11. Expected seasonal variation at SK for the best fitted parameters of the two and three generation LVO solutions to the SNP. We also show in the plot the experimental data points. We have not subtracted the effect of the “normal” seasonal variation (due to $\sim 1/L^2$ dependence) expected in the absence of any oscillation.

which implies that the solar neutrino signals could vary as much as $\sim 7\%$ in one year.

We can see that if vacuum oscillation is assumed, “anomalous” time variation can be expected because the expressions of the probabilities in Eqs. (3), (6), and (7) also dependent on the distance L [14,54,15]. Such “anomalous”

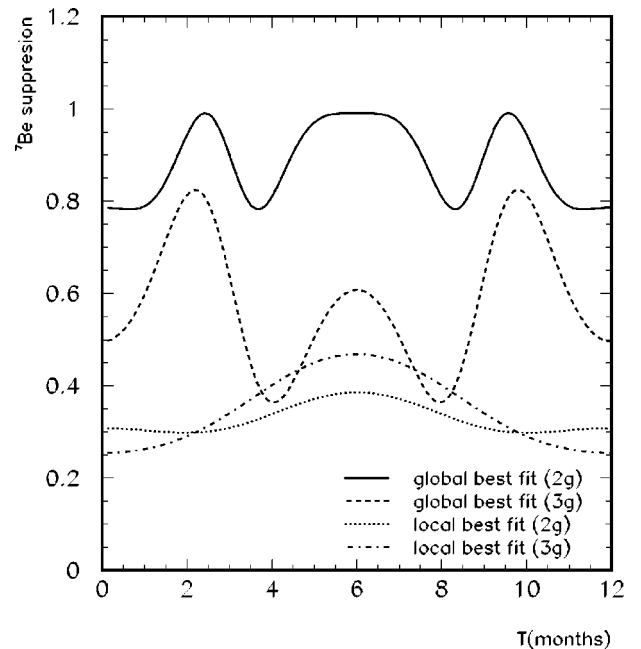


FIG. 12. Same as in Fig. 11 but for Borexino and KamLAND. Here we have subtracted the “normal” seasonal variation due to the $1/L^2$ dependence of the flux.

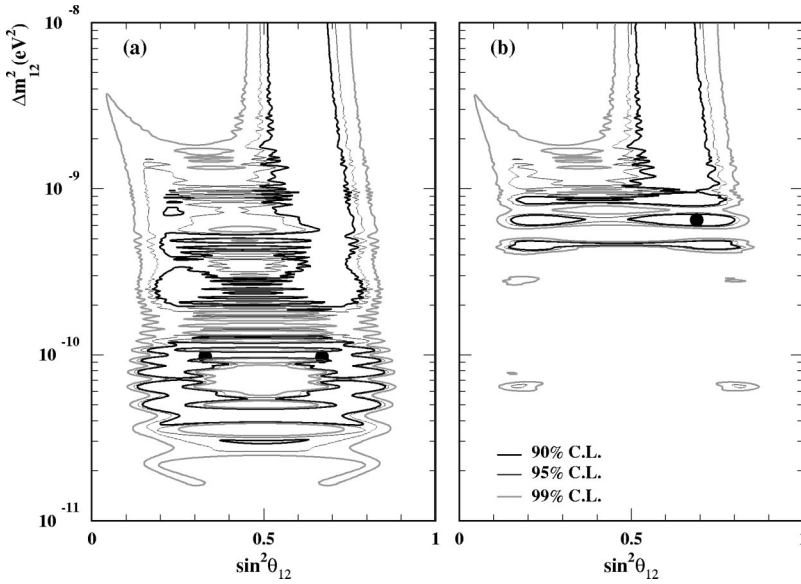


FIG. 13. Region of $(\sin^2 \theta_{12}, \Delta m_{12}^2)$ allowed by (a) the total rates from ^{71}Ga and SK, (b) the combined analysis of rates + SK spectrum in the LVO scenario for two neutrino flavors. The best fit points are shown as a dark circle. Here we have ignored the information from ^{37}Cl .

time variation is expected to be more prominent for ^7Be neutrinos [55]. This is because of the fact that ^7Be neutrinos are monoenergetic at $E=0.862$ MeV (and also at $E=0.383$ MeV, with much smaller flux) with $\Delta E \sim 1$ keV [48], and the oscillation probability of such neutrinos can be very sensitive to the precise value of L , in contrast to the other neutrino fluxes such as pp and ^8B where the probability for these neutrinos must be averaged out over the neutrino energy. Detailed analyses on the seasonal variations for ^7Be neutrinos have been performed in Refs. [49,56,39].

In Fig. 11 we plot the seasonal variation that is expected at SK for the best fitted parameters (global and local) of the two and three generation LVO solutions for $E_e > 5.5$ MeV jointly with the observed SK data [6]. The global and local best fitted parameters correspond to the entries “combined” and “combined (R),” respectively, of Table II, for the two generation, and of Table III, for the three generation solution, with $f_B = 1$ in both cases. SK presents the data without subtracting the expected “normal” seasonal variation due to the $1/L^2$ dependence of the flux. For this reason we have included this extra effect in our curves in Fig. 11. We see that our predictions are currently consistent with the observed SK data.

We also have computed the “anomalous” seasonal variation for the rate of ^7Be neutrino flux at 0.862 MeV that one can expect to be measured by the Borexino [52] and the KamLAND [53] experiments using the best fitted parameters (global and local) for the LVO solution with two and three flavors. Here we have subtracted the expected “normal”

seasonal variation due to the $1/L^2$ dependence of the flux. We note that the predictions for Borexino and KamLAND we have obtained are visually indistinguishable, and therefore, we only plot the case of Borexino in Fig. 12. In this figure our predictions are normalized to the BP98 SSM ^7Be neutrino flux value, i.e., $f_{\text{Be}} = 1$. If f_{Be} is different than unity, our predictions must be renormalized accordingly, keeping the same shape. As we can see from these plots, the best fit for two or three neutrino generations give similar shapes, also large time variation is obtained, which should be observable at both of these experiments. Such drastic variation is due to the fact that the oscillation wavelength for ^7Be neutrinos for our global best fitted values of $\Delta m_{12}^2 = 4.6 \times 10^{-10}$ eV 2 and 6.6×10^{-10} eV 2 , is about 3–4 % of the mean Sun-Earth distance [see Eq. (4)], which is comparable to the Sun-Earth distance variation due to the orbit eccentricity. We have taken into account in our calculations the finite width of the ^7Be line [47]. Such “anomalous” seasonal variation can be a clear signature of the vacuum oscillation, which does not depend on any detail of the SSM nor on unknown experimental systematic errors [39].

VII. ANALYSIS WITHOUT CHLORINE DATA

Finally, in this section, following Refs. [38], we have further investigated the impact of removing from our analysis the chlorine data, since Homestake is the only radiochemical experiment which has not been calibrated with a radioactive source. This is certainly an extreme case but could be worthwhile to be discussed.

TABLE IV. The best fitted parameters and χ_{min}^2 for the two generation LVO solution to the SNP without the chlorine data.

Case	$\Delta m_{12}^2 \times 10^{10}$ eV 2	$\sin^2 \theta_{12}$	f_B	χ_{min}^2	N_{DOF}	C.L. (%)
Rates	0.97	0.33/0.67	1 (fixed)	0.01	1	92.0
Combined	6.5	0.69	1 (fixed)	18.0	23	75.7

TABLE V. The best fitted parameters and χ_{\min}^2 for the three generation LVO solution to the SNP without the chlorine data.

Case	$\sin^2 \theta_{13}$	$\Delta m_{12}^2 \times 10^{10} \text{ eV}^2$	$\sin^2 \theta_{12}$	f_B	χ_{\min}^2	N_{DOF}	C.L. (%)
Rates	0.0	0.97	0.33/0.67	1 (fixed)	0.01	0	
Combined	0.1	4.6	0.76	1 (fixed)	17.4	22	74.1

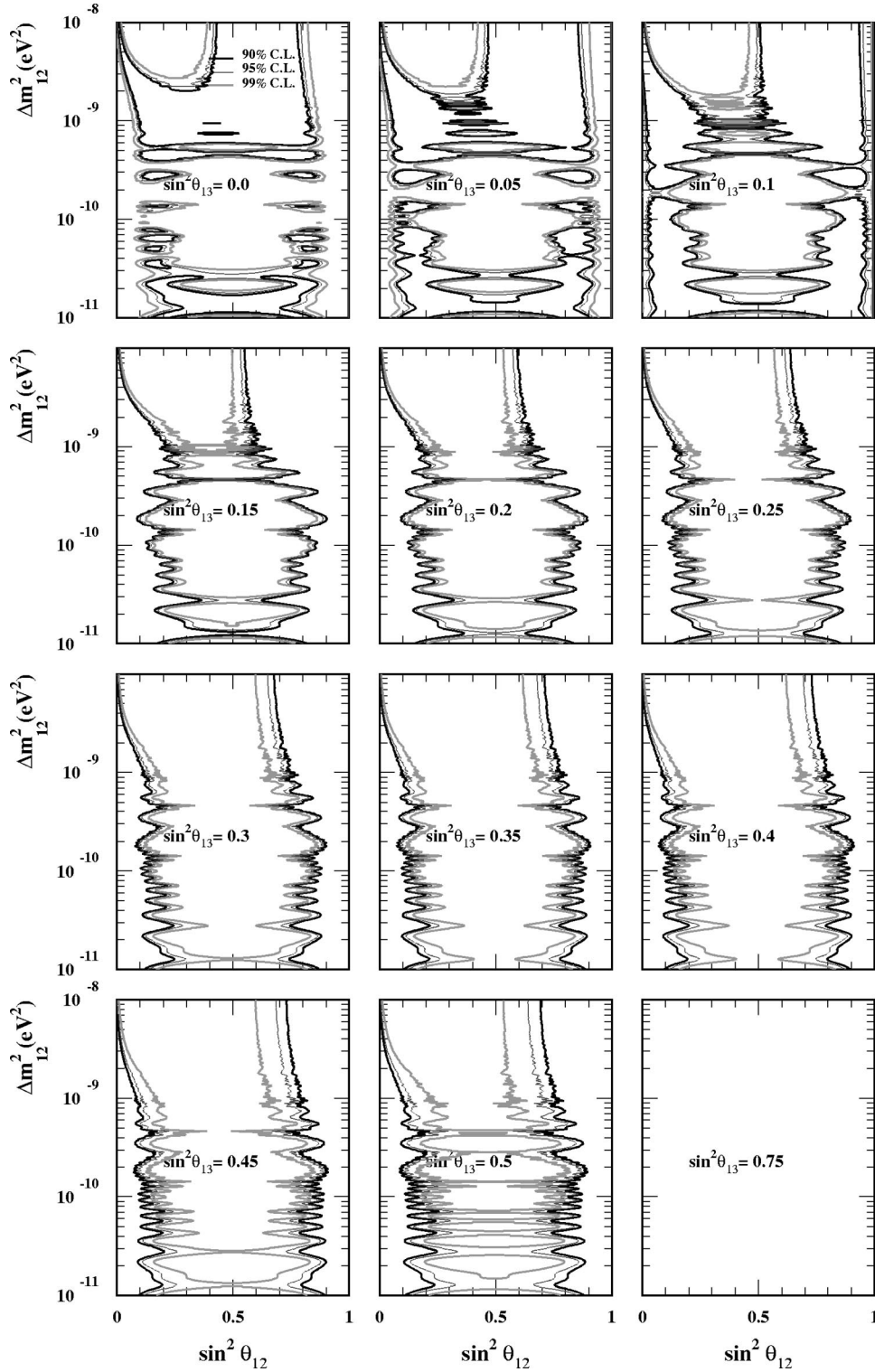


FIG. 14. Region of $(\sin^2 \theta_{12}, \Delta m_{12}^2)$ allowed by the combined analysis of rates + SK spectrum for various values of $\sin^2 \theta_{13}$ for the LVO solution to the SNP with 3 neutrino flavors. Here we have ignored the information from ^{37}Cl .

A. Two generation case

In Figs. 13(a) and 13(b) we show our results for the rates alone and for the combined analysis, respectively, in the case of two generations. We observe here that the rates alone allow for a broader range of solutions in the $\sin^2 \theta_{12} - \Delta m_{12}^2$ plane, compared to Fig. 3(a) where the chlorine data was included, making it more consistent with the SK spectrum measurement. The combined analysis without chlorine data reflects this fact by allowing for larger values of Δm_{12}^2 even at 90 % C.L.

The values of the χ_{\min}^2 as well as of the best fitted parameters here are shown in Tables IV and V. Again the combined χ^2 value also includes χ_{zenith}^2 . We remark that without chlorine data the quality of the combined fit improves since there are significant overlap between the allowed parameter region which give good fit to the total rates and SK spectrum. We can see this by comparing Figs. 2(b) and 13(a). This is in contrast to the case with chlorine data.

B. Three generation case

We repeat the same procedure for the three generation case. In Figs. 14 we show our results for the combined three flavor oscillation analysis, for several values of $\sin^2 \theta_{13}$. Again we see that if one ignores Homestake's data completely a larger range of values of Δm_{12}^2 and $\sin^2 \theta_{12}$ can provide a good explanation for the measured rates as well as for all the solar data combined.

In Fig. 10 we also show the values of $\Delta\chi^2 \equiv \chi^2 - \chi_{\min}^2$ as a function of $\sin^2 \theta_{13}$ for the analysis without ^{37}Cl data. This curve has the same features of the one for the case where all the data was considered in the study, and allows us to put an upper limit on θ_{13} to be less than $\sim 66^\circ$ at 95 % C.L.

VIII. DISCUSSIONS AND CONCLUSIONS

We have reexamined the status of the SNP in the light of the LVO solution, using the most recent solar neutrino data as well as the predictions of the BP98 SSM. We have analyzed the solar neutrino data in the context of two and three neutrino flavor oscillations in vacuum, extending previous analyses to cover the range $10^{-11} \leq \Delta m_{12}^2 \leq 10^{-8} \text{ eV}^2$. In doing this we have included the MSW effect in the Sun, which plays a relevant role in the calculations when $\Delta m_{12}^2/E \geq \text{few} \times 10^{-10} \text{ eV}^2/\text{MeV}$. When we have considered three neutrino generations we assumed a mass hierarchy such that Δm_{13}^2 should be large enough to be relevant for the atmospheric neutrino problem.

We have found that the MSW effect in the Sun significantly modify the allowed parameter space for Δm_{12}^2 larger

than $\sim 3 \times 10^{-10} \text{ eV}^2$ in agreement with the result obtained in Ref. [41]. We, however, found that values of the best fitted parameters are not practically affected by the presence of the solar matter effect (see Table II).

In the two generation LVO solution we found that the rates prefer lower values of Δm^2 , i.e., $\Delta m_{12}^2 \lesssim 3 \times 10^{-10} \text{ eV}^2$ at 90 % C.L., while the SK electron recoil spectrum data excludes such favored parameter region and prefers $\Delta m_{12}^2 \gtrsim 6 \times 10^{-10} \text{ eV}^2$. In the combined analysis the weight of the spectrum prevails.

The disagreement between the best fitted rates and the spectrum predictions for the LVO solution in the case of two generation is, nevertheless, less striking when three neutrinos are considered. When θ_{13} is small, the picture described above applies but as θ_{13} increase the region favored by the total rates are less excluded by the spectrum data compared to the two generation case (see, e.g., Fig. 4 and Fig. 5 for the case $\sin^2 \theta_{13} = 0.15$). When f_B is arbitrary there is even better agreement between spectrum and rates, the regions allowed by them already superpose for $\sin^2 \theta_{13} = 0$.

Judging by the values of the χ_{\min}^2 we have obtained in our combined analyses one could conclude that the LVO solution is in very good agreement with all the solar data. We point out, however, that this fact should be understood as follows: LVO can provide a very good explanation for the spectrum and zenith angle dependence in SK as well as for the total rate of the ^{71}Ga experiments, these are the majority of the statistical points used in our analyses, but provides a poor explanation for the total rates at Homestake and SK. The SK rate can also be well explained if one allows for $f_B \sim 0.74$.

We found that the fit to the total rates as well as SK spectrum are not essentially improved due to the possibility of oscillating into a third neutrino (see Fig. 10). In particular, we obtained the upper bound on θ_{13} to be less than $\sim 60^\circ$ at 95% C.L. by the solar neutrino data alone. We should remark that this bound is substantially weaker than the bound obtained by combining the Super-Kamiokande atmospheric neutrino observations with the CHOOZ reactor experiment limit [24,25]. Hopefully future neutrino oscillation experiments at neutrino factories will be able to give a much more precise information on θ_{13} [57].

Note added: While we were completing this work, we became aware of two similar works [58,59].

ACKNOWLEDGMENTS

We would like to thank Pedro C. de Holanda for useful discussions and Y. Suzuki for providing us with SK data. This work was supported by Fundação de Amparo à Pesquisa do Estado de São Paulo (FAPESP) and by Conselho Nacional de e Ciência e Tecnologia (CNPq).

- [1] J. N. Bahcall, *Neutrino Astrophysics* (Cambridge University Press, Cambridge, England, 1989); for a recent review see also J. N. Bahcall, hep-ex/0002018.
 [2] Homestake Collaboration, K. Lande *et al.*, *Astrophys. J.* **496**, 505 (1998).

- [3] Kamiokande Collaboration, Y. Fukuta *et al.*, *Phys. Rev. Lett.* **77**, 1683 (1996).
 [4] GALLEX Collaboration, W. Hampel *et al.*, *Phys. Lett. B* **447**, 127 (1999).
 [5] V. Gavrin for the SAGE Collaboration, talk given at the ‘‘XIX

- International Conference on Neutrino Physics and Astrophysics (Neutrino 2000),” Sudbury, Canada, 2000, available at URL <http://nu2000.sno.laurentian.ca/V.Gavrin/index.html>
- [6] Y. Suzuki for the Super-Kamiokande Collaboration, talk given at the “XIX International Conference on Neutrino Physics and Astrophysics (Neutrino 2000),” Sudbury, Canada, 2000, available at URL <http://nu2000.sno.laurentian.ca/Y.Suzuki/index.html>
- [7] E. Bellotti for the GNO Collaboration, talk given at the “XIX International Conference on Neutrino Physics and Astrophysics (Neutrino 2000),” Sudbury, Canada, 2000, available at URL <http://nu2000.sno.laurentian.ca/E.Bellotti/index.html>; GNO Collaboration, M. Altmann *et al.*, Phys. Lett. B **490**, 16 (2000).
- [8] J. N. Bahcall, S. Basu, and M. H. Pinsonneault, Phys. Lett. B **433**, 1 (1998); see also Ref. [43].
- [9] For other SSM, see e.g., J. N. Bahcall and R. K. Ulrich, Rev. Mod. Phys. **60**, 297 (1988); V. Castellani *et al.*, Phys. Lett. B **324**, 425 (1994); J. N. Bahcall and M. H. Pinsonneault, Rev. Mod. Phys. **67**, 781 (1995); S. Turck-Chieze *et al.*, Astrophys. J. **335**, 415 (1988).
- [10] See, e.g., H. Minakata and H. Nunokawa, Phys. Rev. D **59**, 073004 (1999), and references therein.
- [11] J. N. Bahcall, M. H. Pinsonneault, S. Basu, and J. Christensen-Dalsgaard, Phys. Rev. Lett. **78**, 171 (1997).
- [12] Z. Maki, M. Nakagawa, and S. Sakata, Prog. Theor. Phys. **28**, 870 (1962).
- [13] S. P. Mikheyev and A. Yu. Smirnov, Yad. Fiz. **42**, 1441 (1985) [Sov. J. Nucl. Phys. **42**, 913 (1985)]; Nuovo Cimento C **9**, 17 (1986); L. Wolfenstein, Phys. Rev. D **17**, 2369 (1978).
- [14] V. N. Gribov and B. M. Pontecorvo, Phys. Lett. **28B**, 493 (1969).
- [15] S. L. Glashow and L. M. Krauss, Phys. Lett. B **190**, 199 (1987); V. Barger, R. J. N. Phillips, and K. Whisnant, Phys. Rev. Lett. **65**, 3084 (1990).
- [16] J. N. Bahcall, P. I. Krastev, and A. Yu. Smirnov, Phys. Rev. D **58**, 096016 (1998); **60**, 093001 (1999).
- [17] M. C. Gonzalez-Garcia, P. C. de Holanda, C. Peña-Garay, and J. W. F. Valle, Nucl. Phys. **B573**, 3 (2000).
- [18] V. Berezhinsky, G. Fiorentini, and M. Lissia, Astropart. Phys. **12**, 299 (2000).
- [19] For earlier MSW analyses, see e.g., N. Hata and P. Langacker, Phys. Rev. D **50**, 632 (1994); G. L. Fogli and E. Lisi, Astropart. Phys. **2**, 91 (1994); J. N. Bahcall and P. I. Krastev, Phys. Rev. D **53**, 4211 (1996).
- [20] For earlier LVO analyses, see e.g., Z. G. Berezhiani and A. Rossi, Phys. Rev. D **51**, 5229 (1995); P. I. Krastev and S. T. Petcov, Phys. Rev. Lett. **72**, 1960 (1994); Phys. Rev. D **53**, 1665 (1996).
- [21] For recent analyses, see e.g., M. M. Guzzo and H. Nunokawa, Astropart. Phys. **12**, 87 (1999); S. Bergmann *et al.*, Phys. Rev. D **62**, 073001 (2000); S. W. Mansour and T. K. Kuo, *ibid.* **60**, 097301 (1999); A. M. Gago, H. Nunokawa, and R. Zukanovich Funchal, Phys. Rev. Lett. **84**, 4035 (2000), and references therein.
- [22] Super-Kamiokande Collaboration, Y. Fukuda *et al.*, Phys. Lett. B **433**, 9 (1998); **436**, 33 (1998); Phys. Rev. Lett. **81**, 1562 (1998); Phys. Lett. B **467**, 185 (1999).
- [23] See for instance: M. C. Gonzalez-Garcia *et al.*, Phys. Rev. D **58**, 033004 (1998); M. C. Gonzalez-Garcia, H. Nunokawa, O. L. G. Peres, and J. W. F. Valle, Nucl. Phys. **B543**, 3 (1999); N. Fornengo, M. C. Gonzalez-Garcia, and J. W. F. Valle, *ibid.* **B580**, 58 (2000).
- [24] G. L. Fogli, E. Lisi, A. Marrone, and G. Scioscia, Phys. Rev. D **59**, 033001 (1999); see also G. L. Fogli *et al.*, Nucl. Phys. B (Proc. Suppl.) **87**, 239 (2000).
- [25] O. Yasuda, in *New Era in Neutrino Physics*, edited by H. Minakata and O. Yasuda (Universal Academic Press, Tokyo, 1999), p. 165; Phys. Rev. D **58**, 091301 (1998); Acta Phys. Pol. B **30**, 3089 (1999).
- [26] CHOOZ Collaboration, M. Apollonio *et al.*, Phys. Lett. B **420**, 397 (1998); *ibid.* **466**, 415 (1999).
- [27] Particle Data Group, C. Caso *et al.*, Eur. Phys. J. C **3**, 1 (1998).
- [28] A. Straessner for the L3 Collaboration, talk given at the XXX-Vth Rencontres de Moriond, 2000, Les Arcs, France; available at URL http://moriond.in2p3.fr/EW/2000/transparencies/6_Friday/pm/Straessner/.
- [29] C-S. Lim, in *Proceedings of BNL Neutrino Workshop*, 1987, New York, USA, edited by M. J. Murtagh, Report No. BNL-52079, C87/02/05, p. 249.
- [30] G. L. Fogli, E. Lisi, and D. Montanino, Phys. Rev. D **49**, 3626 (1994); Astropart. Phys. **4**, 177 (1995).
- [31] T. K. Kuo and J. Pantaleone, Phys. Rev. Lett. **57**, 1805 (1986); Phys. Rev. D **35**, 3432 (1987); Rev. Mod. Phys. **61**, 937 (1989).
- [32] V. Barger and K. Whisnant, Phys. Rev. D **59**, 093007 (1999).
- [33] Z. G. Berezhiani and A. Rossi, Phys. Lett. B **367**, 219 (1996).
- [34] G. L. Fogli, E. Lisi, and D. Montanino, Phys. Rev. D **54**, 2048 (1996).
- [35] G. L. Fogli, E. Lisi, D. Montanino, and A. Palazzo, Phys. Rev. D **62**, 013002 (2000).
- [36] C. Giunti, M. C. Gonzalez-Garcia, and C. Peña-Garay, Phys. Rev. D **62**, 013005 (2000).
- [37] J. N. Bahcall and A. Ulmer, Phys. Rev. D **53**, 4202 (1996).
- [38] A. de Gouvea, A. Friedland, and H. Murayama, hep-ph/0002064.
- [39] A. de Gouvea, A. Friedland, and H. Murayama, Phys. Rev. D **60**, 093011 (1999).
- [40] J. Pantaleone, Phys. Lett. B **251**, 618 (1990).
- [41] A. Friedland, Phys. Rev. Lett. **85**, 936 (2000).
- [42] J. N. Bahcall and P. I. Krastev, Phys. Lett. B **436**, 243 (1998); R. Escribano *et al.*, *ibid.* **444**, 243 (1998); G. Fiorentini *et al.*, *ibid.* **444**, 387 (1998); C. J. Horowitz, Phys. Rev. C **60**, 022801 (1999).
- [43] J. N. Bahcall’s web site at <http://www.sns.ias.edu/~jnb/>. We have used the new BP2000 electron density.
- [44] N. Cabibbo, Phys. Rev. Lett. **10**, 531 (1963); M. Kobayashi and T. Maskawa, Prog. Theor. Phys. **49**, 652 (1973).
- [45] H. Minakata and S. Watanabe, Phys. Lett. B **468**, 256 (1999).
- [46] J. N. Bahcall, M. Kamionkowski, and A. Sirlin, Phys. Rev. D **51**, 6146 (1995).
- [47] J. N. Bahcall, Phys. Rev. D **49**, 3923 (1994).
- [48] J. M. Gelb and S. P. Rosen, hep-ph/9908325.
- [49] B. Faïd, G. L. Fogli, E. Lisi, and D. Montanino, Astropart. Phys. **10**, 93 (1999).
- [50] First paper of Ref. [21].
- [51] G. L. Fogli and E. Lisi, Astropart. Phys. **3**, 185 (1995).

- [52] C. Arpesella *et al.*, BOREXINO proposal, Vols. 1 and 2, edited by G. Bellin *et al.* (University of Milano, Milano, 1991); R. S. Raghavan, *Science* **267**, 45 (1995); see also URL <http://www.lngs.infn.it/site/exppro/borex/borexino.htm>
- [53] A. Suzuki, for the KamLAND Collaboration, *Nucl. Phys. B (Proc. Suppl.)* **77**, 171 (1999); see also URL <http://www.awa.tohoku.ac.jp/html/KamLAND/index.html>
- [54] V. Barger, R. J. N. Phillips, and K. Whisnant, *Phys. Rev. D* **24**, 538 (1981).
- [55] S. Pakvasa and J. Pantaleone, *Phys. Rev. Lett.* **65**, 2479 (1990).
- [56] P. I. Krastev and S. T. Petcov, *Nucl. Phys.* **B449**, 605 (1996).
- [57] See, e.g., S. Geer, *Phys. Rev. D* **57**, 6989 (1998); **59**, 039903(E) (1999); A. De Rujula, M. B. Gavela, and P. Hernandez, *Nucl. Phys.* **B547**, 21 (1999); V. Barger, S. Geer, and K. Whisnant, *Phys. Rev. D* **61**, 053004 (2000).
- [58] C. E. C. Lima and H. M. Portella, hep-ph/0005053.
- [59] G. L. Fogli, E. Lisi, D. Montanino, and A. Palazzo, *Phys. Rev. D* **62**, 113004 (2000).